AN INVESTIGATION OF COMPRESSIBLE FLOWS WITH LARGE WHIRL COMPONENTS

ROBERT LEE BOSHOVEN

[redacted]

AN INVESTIGATION OF COMPRESSIBLE FLOWS WITH LARGE WHIRL COMPONENTS

by

Robert Lee Boshoven
Lieutenant, United States Navy
B.S., University of Michigan, 1959

Submitted in partial fulfillment of the
requirements for the degree of

AERONAUTICAL ENGINEER

from the

NAVAL POSTGRADUATE SCHOOL
June 1967

ABSTRACT

This investigation was conducted to determine the losses in the scroll and inlet guide vanes of a dual discharge, radial-inflow turbine. Difficulties are encountered in such tests because the air is discharged from the guide vanes with a large whirl component into the cavity normally occupied by the turbine rotor. Connected with such flows are phenomena such as choking and energy separation. This led to the investigation of the flow in a vortex chamber where the vortex is driven by the inlet guide vanes of the radial turbine.

The air tests were conducted at the Turbo-Propulsion Laboratory of the Naval Postgraduate School, Monterey, California.

TABLE OF CONTENTS

LIST OF ILLUSTRATIONS

FIGURE PAGE

TABLE OF SYMBOLS

Actual	Definition	FORTRAN	Units
A_1	Meridional cross-sectional area at dummy rotor inlet	A1	ft^2
A_δ	Cross-sectional area of scroll without friction		in^2
$A_{\delta f}$	Cross-sectional area of scroll corrected for friction		in^2
A_5	Cross-sectional area of five-inch pipe		ft^2
a	Acoustic velocity		ft/sec
a_i	Acoustic velocity at radius R_i		ft/sec
B_1	Distance between turbine rotor shrouds at dummy rotor inlet	B1	in
b	Width of vortex chamber		in
C	Factor dependent on orifice diameter and type of pressure taps used		
C_f	Conversion factor	CF1	lb/ft^2/ in Hg
c	Constant defined in Appendix B		ft
c_p	Specific heat at constant pressure	CP	BTU/ lb_m ^oR
F	Scale reading	SR	lb
F_r	Reynolds number correction factor		
f	Skin friction coefficient		
G_{Hg}	Specific Gravity of mercury at t_{rm}	GHG	

Actual	Definition	FORTRAN	Units
G_{H2O}	Specific gravity of water at t_{rm}	GWR	
g	Gravitational constant	32.174	lb_m-ft/ lb-sec^2
h_{atm}	Measured atmospheric pressure	HATM	in H_2O
h_1	Average measured pressure at dummy rotor inlet	H1	in H_2O
h	Measured pressure as appropriate		in H_2O
h_{ref}	Measured static pressure in five-inch pipe		in H_2O
h_{1vc}'	Measured pressure across orifice (vena contracta taps)	DPVC	cm Hg
Δh_{1vc}	Actual pressure across orifice (vena contracta taps)	DVC	
J	Conversion factor	778.16	ft-lb/Btu
M	Mach number		
M	Moment exerted on dummy rotor	M	ft-lb
M_i	Mach number at radius R_i		
M_r	Ratio of measured dynamic pressure to measured absolute total pressure for probe calibration		
M_1	Mach number at dummy rotor inlet	ACH1	
MV_4	Thermocouple reading ahead of orifice	V4	mv
MV_5	Thermocouple reading at manifold inlet	V5	mv
P_{atm}	Atmospheric pressure (barometer)	PAT	in Hg

Actual	Definition	FORTRAN	Units
P_t	Total pressure as appropriate		
P_{to}	Total pressure at manifold inlet	PTO	in Hg abs
P_{t2}	Total pressure at rotor discharge section		in Hg abs
p	Absolute static pressure as appropriate		
p_i	Absolute static pressure at radius R_i		
p_o	Absolute static pressure at manifold inlet	PS5	cm Hg abs
p_1	Average static pressure at dummy rotor inlet	P1	in Hg
p_2	Actual static pressure at rotor discharge section		cm H_2O
p_5'	Measured static pressure at manifold inlet	P5P	cm Hg gage
p_{1vc}'	Measured pressure upstream of orifice (vena contracta taps)	PUVC	cm Hg gage
p_{1vc}	Absolute pressure ahead of orifice (vena contracta taps)	PVC	cm Hg abs
P_{to}/p_1	Ratio of total pressure at manifold inlet to static pressure at dummy rotor inlet	PR	
P_1-p_2	Measured dynamic pressure		cm H_2O
p_4-p_5	Measured pressure difference between the two pitch angle pressure taps		cm H_2O
$\frac{P_1-P_t}{P_t-p_s}$	Total pressure coefficient		

Actual	Definition	FORTRAN	Units
$\frac{p_4-p_5}{P_1-p_2}$	Pitch angle pressure coefficient		
$\frac{P_t-p_s}{P_1-p_2}$	Velocity pressure coefficient		
P_t-p_s	Actual dynamic pressure		cm H_2O
R	Radius as appropriate		
R_1	Radius at dummy rotor inlet		ft
R_i	Injection radius where conditions M_i and α_i are known		ft
R_o	Rotor shroud radius at rotor discharge section		in
r	Radius of scroll cross-sectional area		ft
r_1	Inside radius of scroll		ft
r_f	Radius of scroll cross-sectional area corrected for friction		ft
T	Static temperature		^oR
T_i	Static temperature at radius R_i		^oR
T_t	Total temperature as appropriate		^oR
T_{to}	Total temperature at manifold inlet	T5	^oR
T_o	Static temperature at manifold inlet	TO	^oR
T_{t2}	Total temperature at rotor discharge section		^oR
T_1	Static temperature at dummy rotor inlet	T1	^oR
T4	Temperature ahead of orifice	T4	^oR

Actual	Definition	FORTRAN	Units
t	Temperature as appropriate	A	^{o}F
tare	Tare of mercury micro-manometer	TARE	cm Hg
tare	Tare of precision scale	STARE	lb
t_{cj}	Cold junction temperature	TCJ	^{o}F
t_{rm}	Control room temperature	TRM	^{o}F
V	Velocity		ft/sec
V_i	Velocity at radius R_i		ft/sec
V_m	Meridional velocity component		ft/sec
V_o	Velocity at manifold inlet	V1 (VO?)	ft/sec
V_{mi}	Meridional velocity component at radius R_i		ft/sec
V_u	Peripheral velocity component		ft/sec
V_{ui}	Peripheral velocity component at radius R_i		ft/sec
V_1	Velocity at dummy rotor inlet	V1	ft/sec
V_{1th}	Theoretical velocity at dummy rotor inlet		ft/sec
V_{m1}	Meridional component of V_1	VM1	ft/sec
V_{u1}	Peripheral component of V_1	VU1	ft/sec
V_2	Velocity at rotor discharge section		ft/sec
$V_{\delta 1}$	Tangential velocity component at inside radius of scroll		ft/sec
$\mathcal{V}$	Volume flow rate		ft^3/sec
$\dot{W}_{vc}$	Mass flow rate (vena contracta taps)	WVC	lb_m/sec
X	Reynolds number factor	X	

Actual	Definition	FORTRAN	Units
Y_1	Expansion factor accounting for thermal expansion of orifice	Y	
Z	Absolute viscosity		centi-poises
Ƶ	Axial coordinate in vortex chamber measured from center plane	Ƶ	in
α	Area multiplier accounting for thermal expansion of orifice	A	
α	Flow angle		degrees
α_i	Flow angle at radius R_i		degrees
α_1	Absolute dummy rotor inlet flow angle	ALP1	degrees
α_2	Measured yaw angle of flow at rotor discharge section		degrees
γ	Ratio of specific heats	GAM	
$\frac{\gamma-1}{\gamma}$	Exponent using γ	EXP	
δ	Circumferential angle of advance of scroll measured from inlet pipe centerline		degrees
Δq	Nondimensional pressure loss in scroll		
ϕ	Velocity coefficient of scroll and guide vanes	PHI	
ρ	Density		lb_m/ft^3
ρ_i	Density at radius R_i		lb_m/ft^3
ρ_o	Density at manifold inlet	RHO	lb_m/ft^3
ρ_1	Density at dummy rotor rotor inlet	RHO	lb_m/ft^3
θ_2	Measured pitch angle of flow at rotor discharge section		degrees

1. Introduction

For axial turbine stages it is possible to determine, at least in a fairly accurate manner, the losses in guide vanes by passing air through the axial cascade with the rotor removed. Nevertheless, errors occur if blade heights are large with respect to the blading diameter. These errors are due to the fact that the rotor blading will set up radial pressure gradients after the guide vanes so that the guide vanes will not discharge into a constant pressure region as they do in tests with rotor removed.

If the guide vanes of a radial turbine are tested with the rotor removed, conditions exist which make direct measurements of the required parameters difficult. Large whirl components of velocity are produced after the inlet guide vanes in the cavity which would normally be occupied by the turbine rotor. These whirl components increase with decreasing radius if angular momentum is conserved. This whirling flow may lead to such phenomena as choking and energy separation. Flow conditions may then be completely different in the vaneless space after the guide vanes than with the turbine rotor installed. Vavra [1][1] has surveyed the discharge of the inlet guide vanes of a radial turbine and determined that it was possible to measure a higher total pressure after the guide vanes than was known to exist before them. This seems to be in violation of the principle of the conservation of energy. It was also determined that a

1 Numbers in brackets refer to bibliography entries of section 8.

considerable vacuum core existed near the centerline causing ambient air to flow in and mix with the discharge air of the guide vanes. It seemed possible that this effect and the interesting but not well understood phenomenon known as the "Ranque-Hilsch effect" might be connected with the experienced conditions.

The subject investigation was undertaken to determine losses in the scroll and inlet guide vanes of a radial turbine and to better understand the conditions existing in the flow after the guide vanes with the turbine rotor removed.

Riley [2] has investigated the effect of axial clearance on the performance of a radial turbine and found that the efficiency of the turbine remained relatively constant until a "critical" clearance was reached beyond which point a further increase in clearance caused the efficiency to decrease rapidly. In determining some performance parameters it was assumed that the velocity coefficient, which is a measure of the losses occurring in the inlet manifold and guide vanes, as well as the absolute rotor inlet angle, were constant in the range of turbine pressure ratio and axial clearance tested. It was desired to conduct more extensive tests of the inlet manifold and guide vanes so that a more definitive analysis of Riley's data could be made. If the investigation led to the possibility of improvements in the existing installation, these would be incorporated before future turbine tests were conducted.

Essentially four separate but related investigations were carried out. Conditions at the rotor inlet and losses in the inlet manifold and guide vanes were evaluated from dummy rotor torque tests. A computer program was used to reduce data and calculate the desired parameters from these tests. Surveys were conducted to determine the flow conditions in the plane of the turbine rotor discharge with the rotor removed. Pressure measurements were made around the periphery of the radial turbine inlet manifold to ascertain whether the scroll could be improved. The turbine rotor shrouds were replaced with flat plates which formed vortex chamber sides, and an investigation of the flow in the vortex chamber was conducted.

Whirling flows have increased in importance not only in the field of radial or mixed-flow turbines and compressors, but also in studies relating to spin stabilized solid propellant rockets, particle separators, and gaseous nuclear rockets.

The author gratefully acknowledges the assistance and encouragement given by Dr. M. H. Vavra of the Department of Aeronautics.

2. General Installation and Instrumentation

The same basic installation was used in all the subject investigations, with some changes in components and instrumentation for the different tests. It consisted of the scroll type inlet manifold and the inlet guide vanes of a dual discharge, radial-inflow turbine. The unit is located at the Turbo-Propulsion Laboratory of the Department of Aeronautics at the Naval Postgraduate School. The scroll type inlet manifold is of laminated wood with the inner contour formed by casting plaster of Paris around a wooden insert. This insert which is in the shape of a scroll or torus of varying cross-sectional area is shown in Fig. 1. The manifold casing which was constructed in halves has been sanded and varnished internally to provide a smooth flow surface and to prevent erosion. The seven inlet guide vanes which have circular arc profiles are held between two rings, which are in turn fastened to the manifold casing when it is assembled. Fig. 2 is a cross section of the manifold casing showing the scroll shape and inlet guide vane positions.

The source of air for all tests is an Allis-Chalmers 12-stage axial flow compressor which provides high pressure air for the three test cells at the Turbo-Propulsion Laboratory. Air from the main supply line passes through a four-inch pipe with a flow-measuring orifice, a settling tank, and a five-inch pipe with flow straighteners, before entering the turbine inlet manifold. The flow rate is regulated from the control room by two remotely controlled butterfly valves which are shown in Fig. 3.

A sharp-edged orifice, which conforms to standards set forth by Stearns, et al. [3], is located in the four-inch pipe which is shown in Fig. 3. The pressure ahead of the orifice and the pressure difference across the orifice were obtained with standard flange and vena contracta taps. A chromel-alumel thermocouple installed in a Kiel temperature probe was used to measure the temperature ahead of the orifice.

Thermocouple voltage potentials were measured on a 48 channel Brown Potentiometer manufactured by Minneapolis Honeywell. The potentiometer shown in Fig. 4 is located in the control room. The reference or cold junction temperature is maintained at 32°F by an ice bath in the test cell.

The pressures obtained from the vena contracta and flange taps of the flow-measuring orifice, and the wall static pressure in the five-inch pipe at the manifold inlet, were measured with an accuracy of $\pm$ 0.01 cm. on a 100 cm. mercury micromanometer in the control room. The wall static pressure in the five-inch pipe at the manifold inlet can also be read on a Heise pressure gage in the control room. The Heise gage is shown in Fig. 4. This gage was usually used to set the pressure ratio for test runs. When it was desired to set the same conditions in different test runs as nearly as possible, the mercury micromanometer was used to reset the wall static pressure in the five-inch pipe. The total pressure and total temperature were sensed at the manifold inlet at the centerline of the five-inch pipe with a Kiel probe containing a chromel-alumel thermocouple.

A 96-inch water manometer board in the control room was used to measure static pressures around the scroll periphery, the static pressures ahead of the inlet guide vanes, and the static pressures after the inlet guide vanes or in the vortex chamber side walls depending on the test. The pressure heads were measured with an accuracy of $\pm$ 0.05 inches. Atmospheric and/or wall static pressures in the five-inch pipe were used as reference pressures for the reservoirs of the 96-inch manometer board.

Equipment and instrumentation not utilized in all tests are described separately in the sections concerning the test to which they are applicable.

3. Scroll and Guide Vane Performance from Torque Measurements

Installation

Because difficulties were encountered in attempting to evaluate the inlet guide vane discharge conditions from pressure surveys, Vavra [1] and subsequently Riley [2] used a special installation to determine the losses in the scroll and guide vanes as well as the absolute flow angle at the rotor inlet. This installation actually determines average conditions at a position which would normally be the rotor inlet radius, thereby including changes in the flow conditions in the vaneless space between the inlet guide vanes and the rotor. This information may be more useful in the determination of performance parameters. It was desired to make improvements to the installation and to conduct more extensive tests especially to investigate the effect of increased axial clearance on this method of performance determination.

A dummy rotor with 36 meridional blades that approximate the contour of the turbine rotor shrouds is supported on self-aligning ball bearings and replaces the turbine rotor. The dummy rotor turns the flow that is discharged by the guide vanes to the axial direction at the rotor discharge. If the flow leaves the rotor with no peripheral velocity component, it is possible to determine the losses in the guide vanes by measuring the torque exerted on the static dummy rotor, the flow rate, the conditions at the manifold inlet, and the static pressure at the dummy rotor inlet. The dummy rotor shown in Fig. 5 has a diameter of 9.50 inches. This places the blade leading edges at the radius which corresponds with the radius of the annulus in which the static pressure taps ahead of the rotor are located, and at a 0.050 inch greater radius than the actual rotor inlet. The pressure taps depicted in the cross section in Fig. 6 are placed at eight equidistant positions around the periphery of the so-called right-hand side and left-hand side plexiglas rotor shrouds. A total of sixteen pressure taps are individually connected to the 96-inch water manometer board. The axial length of the dummy rotor is 8.50 inches, which extends the blade trailing edges beyond the shrouds shown in Fig. 6.

To insure that the discharge flow was without whirl components, new flow straighteners were fabricated and attached to the dummy rotor for these tests. The flow straighteners shown in Fig. 5 are aluminum caps which slide over the rotor shaft and cover the rotor blade trailing edges. The caps contain a 1.00 inch depth of 0.125 by 0.0015 inch honeycomb material to insure an axial discharge.

The entire dummy rotor assembly is supported by brackets attached to the manifold casing as shown in Fig. 7. The rotor was centered in the shrouds with shims so that there was a uniform radial clearance at the discharge of 0.035 inches. The axial clearance was varied in individual test runs by placing circular shims or gaskets between the shrouds and the manifold casing. A twelve-inch lever arm was attached to the rotor shaft so that the moment exerted on the dummy rotor by the flow could be measured with a 25-pound capacity Toledo precision scale. The lever arm is attached horizontally and the force is exerted on the scale through an exactly vertical link so that scale readings and moment are directly related. To extend the capacity of the scale and to allow tests at higher pressure ratios (and mass flow rates) a counterbalance was added to the lever arm. The installation for these tests is shown in **Fig. 7**.

Analytical Derivation and Data Reduction

The integrated pressures acting over the inlet and discharge areas of the dummy rotor cannot produce a moment about the axis. The flow straighteners insure that the discharge velocity is axial. Then from the law of moment of momentum[1], for a steady flow that does not have a peripheral velocity component at the discharge section, the moment M exerted on the dummy rotor is

$$M = \frac{\dot{W}_{vc}}{g} R_1 V_{u1} \qquad (3\text{-}1)$$

where $\dot{W}_{vc}$ is the mass flow rate determined by using the vena contracta taps of the flow measuring orifice. R_1 is the radius at the inlet of the dummy rotor and V_{u1} is the peripheral velocity component at R_1. The velocity coefficient ϕ, which is a measure of the performance of the

[1]Vavra, M. H. Aero-Thermodynamics and Flow in Turbomachines (John Wiley and Sons, 1960), p. 98.

scroll and inlet guide vanes, is defined by

$$\phi \equiv \frac{V_1}{V_{1th}} \tag{3-2}$$

where V_1 is the actual average velocity at the dummy rotor inlet section and V_{1th} is the theoretical velocity for an isentropic expansion from the manifold inlet conditions P_{to}, T_{to} to the static pressure p_1 at the dummy rotor inlet. From the energy equation for an adiabatic process, the velocity V_1 at the dummy rotor inlet is

$$V_1 = \sqrt{2g\,Jc_p\,(T_{to} - T_1)} \tag{3-3}$$

or using the isentropic relation for a perfect gas and equation (3-3),

$$V_1 = \phi\,\sqrt{2g\,Jc_p\,T_{to}\left[1-\left(\frac{p_1}{P_{to}}\right)^{\frac{\gamma-1}{\gamma}}\right]} \tag{3-4}$$

From the equation of continuity, expressed at the dummy rotor inlet, the average meridional component of velocity V_{m1} is

$$V_{m1} = \frac{\dot{W}_{vc}}{\rho_1 A_1} \tag{3-5}$$

where A_1 is the meridional cross section and ρ_1 the density at the dummy rotor inlet. The area, A_1, is

$$A_1 = 2\pi R_1 B_1 \tag{3-6}$$

where B_1 is the distance between the shrouds at the dummy rotor inlet which varies with the set axial clearance. From the equation of state for a perfect gas, the density ρ_1, is

$$\rho_1 = \frac{p_1}{R_g T_1} \tag{3-7}$$

Then the meridional velocity V_{m1} is

$$V_{m1} = \frac{\dot{W}_{vc} R_g T_1}{A_1 p_1} \qquad (3\text{-}8)$$

The velocity V_1 is

$$V_1 = \sqrt{V_{m1}^2 + V_{u1}^2} \qquad (3\text{-}9)$$

Equations (3-3), (3-4) and (3-9) are expressions for the velocity V_1, which after the substitution of equations (3-1) and (3-8) into equation (3-1) will have three unknowns. The unknown quantities to be determined are the velocity V_1, the velocity coefficient ϕ, and the temperature T_1. All other quantities are either constants or quantities determined directly from measured data. The computer program SCROLL which is described in detail and listed in Appendix A determines the unknowns from test data using an iteration process. With the velocity components determined, the absolute flow angle at the dummy rotor inlet is

$$\alpha_1 = \tan^{-1} \frac{V_{u1}}{V_{m1}} \qquad (3\text{-}10)$$

Program SCROLL makes temperature corrections to the physical properties of air and the specific gravity of water and mercury used in the respective manometers. It converts manometer readings and thermocouple outputs into the required pressures and temperatures, respectively. The program then establishes the mass flow rate and calculates the average conditions at the dummy rotor inlet from the torque measurement. The program was processed on the Control Data Corporation 1604 Computer at the Naval Postgraduate School.

Testing and Results

A total of five test runs were completed. Program SCROLL input and output data for these runs are tabulated in Appendix A. The velocity coefficient and flow angle as functions of pressure ratio are shown graphically in Fig. 8, 9 and 10. Data for a single test run made by Riley [2] are also shown.

The initial test run was conducted at minimum axial clearance but with the flow straighteners installed. Because the pressures p_1 at the dummy rotor inlet are sensed at sixteen positions, Polaroid photographs were used to record the manometer board. The pressure heads were averaged for use in program SCROLL. Velocity coefficients near the design point pressure ratio of the turbine are approximately two percentage points higher for this first run than those determined by Riley [2]. This seemed to indicate that the addition of flow straighteners eliminated any peripheral velocity components at the discharge which may have existed with the former installation.

For the second run circular aluminum shims of 0.030 inch thickness were placed between the shrouds and the manifold casing. With this increased axial clearance, the resulting velocity coefficients were about one percentage point lower than with the minimum clearance in the range of interest.

During the first two test runs it was observed that the static pressures measured at the dummy rotor inlet varied considerably from position to position around the periphery of the shroud. They were also observed to be sensitive to the relative positions of the rotor blade leading edges. To reduce the effects of local perturbations, the pressure tap positions were moved axially outward in the annulus around the periphery of the shroud. To prevent leakage between the shrouds and manifold casing 0.015 inch thick circular gaskets were placed there for the third run. This effectively increased the axial clearance by the thickness of the gasket. The repositioning of the pressure taps greatly improved the uniformity of pressures sensed around the shrouds.

The velocity coefficients resulting from the third run were larger than in the preceding runs. This may indicate that the static pressures recorded were nearer to actual average conditions existing at the rotor inlet. The pressure ratio P_{to}/p_1 was thereby reduced and the theoretical velocity V_{1th} decreased correspondingly, thus increasing the resulting velocity coefficients ϕ for the same flow conditions.

It was noted in the first three runs that pressures sensed on the right side were somewhat greater than those on the left. Measurements showed that the inside extremity of the left shroud was offset 0.016 inch more from the guide vane ring than the right shroud. The dummy rotor was centered between the shrouds for all runs. To improve the symmetry of conditions in the final runs, a greater thickness of gasket material was placed between the right shroud and the manifold casing.

In an attempt to eliminate influences other than dummy rotor axial tip clearance, run No. 5 was conducted immediately following run No. 4. The only change to the installation between these runs was the reduction of the axial clearance by 0.025 inch by the removal of a 0.025 inch thick gasket from under each shroud. The clearances were 0.072 and 0.047 inch for runs 4 and 5 respectively. The data from run 5 compares very well with that from run 3, which was conducted at a 0.051 inch clearance. The velocity coefficient near design pressure ratio determined by runs 3 and 5 is approximately 92.5 percent. The clearances set for runs 1 and 2 were 0.036 and 0.066 inch, respectively. A comparison of runs 1 and 2 and of runs 4 and 5 indicates that an increase in axial clearance, of the amounts made, decreases the velocity coefficient by approximately one percent. An explanation of this may be that the angular momentum of the flow escaping around the blade tips is decreased by wall friction before it impinges on the dummy rotor blades at a lesser radius. It appears then that the most accurate performance would be obtained from the type of test conducted where the blade profile conforms closely to the shroud contour and where the axial clearance is minimized near the dummy rotor blade tips.

Riley [2] used a distance of 0.943 inch between the shrouds at the rotor inlet for his analysis. Since the axial width of the blade tips of the dummy rotor is 0.894 inch, this would indicate that there existed an axial clearance of 0.0245 inch. The axial clearances in the subject tests were larger than in Riley's test because the distance between shrouds was determined to be 0.966 inch without gaskets or shims installed. The axial clearance set in the different tests ranged from a minimum of 0.036 inch to 0.072 inch. Since the manifold casing had been disassembled and varnished internally after Riley's test, the distance between the shrouds probably changed. The wooden manifold casing is also subject to changes in dimensions with changes in atmospheric humidity.

The axial distance between the shrouds has a limited effect on the calculation of the velocity coefficient; however, since it is used directly in calculation of the meridional velocity component from the mass flow rate, it influences the rotor inlet angle α_1 considerably. The decrease in α_1 in runs 1 and 5 in Fig. 10 is in the main due to the increase in the calculated meridional velocity component for a decrease in the distance between shrouds. In any given run α_1 decreases with increasing pressure ratio due to the requirement that it decreases with increasing mass flow rate.

Fig. 8 and 9 indicate that the velocity coefficient increases slightly with increasing pressure ratio. If the internal surfaces are smooth enough, this result may be due to a decreasing coefficient of friction with increasing Reynolds number.

Conclusions and Recommendations

The velocity coefficient ϕ for the inlet manifold and guide vanes is at least 92.5%. If the axial tip clearance could be reduced to a minimum while maintaining the rotational freedom of the dummy rotor, it is possible that an increased velocity coefficient would be determined indicating that the losses are in reality lower. This would require reworking the dummy rotor or turbine rotor shrouds.

Future testing of the radial turbine should be conducted using the static pressure taps at the rotor inlet in their new location in order to obtain more reliable data at this position.

4. Survey of Turbine Rotor Discharge Section with Rotor Removed

Because peculiar conditions such as extreme noise and high frequency vibrations exist if tests are carried out with the turbine rotor removed, this configuration was investigated to gain some insight into the existing flow conditions. The installation had been equipped to allow pressure and temperature surveys of the flow at the turbine rotor discharge in earlier turbine performance tests. Using the available instrumentation, the rotor discharge area was surveyed with the rotor removed. Because working at a higher pressure ratio was almost impossible due to the extreme noise and vibrations, a survey of the discharge area was conducted at $\frac{P_{to}}{P_{atm}} = 1.25$ only. The flow was assumed to be axisymmetric and the pressure and temperature surveys were conducted at one peripheral position, but 90 degrees apart. The axial position of the survey plane at the discharge is shown in Fig. 6.

A United Sensor Model DA-120 pressure probe was used to survey the discharge section. This instrument is a three-dimensional pressure probe capable of measuring the yaw and pitch angles, and total and static pressures. The probe holder was mounted on the upper surface of the inlet casing, and the probe passes through the casing and the shroud as shown in Fig. 6. The probe can be moved vertically and rotated about the vertical axis. Yaw angles are determined by rotating the probe to balance static pressures sensed on either side of the wedge of the probe. With the measured pressure differential sensed by the axially spaced taps, 4 and 5, shown in Fig. 11, the pitch angle is determined from calibration curves for the probe. All pressures sensed by the probe were measured differentially on the U-tube water manometer board shown in Fig. 21. The probe is connected to the manometer board as shown in Fig. 12.

The total temperature probe used to survey the discharge section is depicted in Fig. 11. This probe, which utilizes an iron-constantant thermocouple, was manufactured locally. It was mounted on the end of the manifold casing in a holder similar to that used for the pressure probe. The temperature probe is located in the same axial plane but at a peripheral position 90° away from the pressure probe. The temperature probe was set at the same radial positions and yaw angles that were obtained by the pressure probe. The thermocouple output was measured on the potentiometer in the control room.

The results of the pressure and temperature surveys are shown graphically in Fig. 13 through 16. From the pressure distribution at the section surveyed it is apparent that the discharge flow is confined to the area where the radius ratio is between 0.75 and 1.00. This area is approximately 43% of the total cross-sectional area. The central core was at a pressure below the atmospheric pressure with velocities either nonexistent or of magnitudes too small to establish reliable differential pressure information. The largest velocities exist at the outer radius near the surface of the shroud. The velocity distribution was established by assuming isentropic recovery of total pressure by the probe. Since the total temperature was also measured, there is from the energy equation for an adiabatic flow,

$$V_2 = \sqrt{2gJc_p T_{t2}\left[1 - \left(\frac{P_2}{P_{t2}}\right)^{\frac{\gamma-1}{\gamma}}\right]} \qquad (2\text{-}1)$$

The velocity distribution is shown in Fig. 16. The yaw angle shown in Fig. 14 is nearly constant in the range from $R/R_o = 1.0$ to $R/R_o = 0.9$, indicating that the axial and peripheral velocity profiles are similar. However at smaller radius ratios the flow turns considerably toward the axial direction.

The pitch angle distribution determined from the survey is shown in Fig. 14 also. The high pitch angles close to the shroud surface are considered to be in error. The determination of pitch angle is dependent upon the calibration curves which are obtained for deeply immersed probes. If measurements are made close to the wall the uppermost tap of the two pressure sensing taps is inside the probe access hole. Large pitch angles close to the wall are inconsistent with the physical situation. Because the static pressure is also dependent upon the calibration curves through the pitch angle, the calculated velocities shown in Fig. 16 may be too high near the shroud surface.

The largest velocities at a given pressure ratio can be expected to occur at the point of maximum curvature of the meridional shroud contour before the flow is turned into the axial direction. From the survey it appears that all velocities are well below the acoustic velocity at the pressure ratio of the test. Nevertheless the noise and vibration level were extremely high and almost unbearable. The frequencies and amplitudes of the vibrations increased with increasing pressure ratio. Although the flow seemed to be stable from an overall point of view, the low pressure core seemed somewhat unstable and irregular. If smoke was released into the core from the outside it was sometimes carried up into the shrouds and sometimes it was ejected axially through the opposite side. Since the distance between shrouds increases rapidly with decreasing radius due to the curvature of the shrouds, the flow will decrease its radial velocity components considerably as it moves toward the axis. It may be possible that the flow midway between the shrouds approaches a solid body rotation without radial velocity components. A secondary flow condition may even exist with radial inward velocity components at the walls of the shrouds and radial outward velocity components midway between them. Such a rotating flow may extend radially outward to the inlet guide vanes and impose an unsteady condition as it passes the seven individual guide vanes or produce nonuniform pressure distributions in the scroll.

It might be of interest to determine the change of the frequencies of the vibrations with pressure ratio or flow rate, to verify whether a correlation exists between the frequency of vibration and the rotational velocity of the flow.

5. Scroll Performance

The turbine inlet manifold is described in section 3. It has a complex, three-dimensional shape that makes an analytical study of the flow difficult. The shape of the scroll is depicted in Fig. 1 and 2. The purpose of the scroll is to produce a uniform flow with constant static and total pressure ahead of the inlet guide vanes. The average velocity would then be constant at the leading edges of the guide vanes everywhere on the periphery. With losses however both conditions cannot be realized and a uniform static pressure around the periphery may be the more important criteria. A constant pressure around the periphery prevents the rotor from experiencing varying forces and radial thrust. Unbalanced flow may accelerate the wear of bearings and seals. To accomplish the desired conditions the cross-sectional area of the scroll must decrease with the angle of advance. If the flow in the scroll is considered frictionless, angular momentum is conserved and the velocity increases with decreasing mean radius. This effect will be reduced somewhat by wall friction. The effects of friction and the displacement thickness of the boundary layer require that cross-sectional areas be increased over those for frictionless flow. Due to the complexity of the flow, the loss in angular momentum is usually neglected and the blockage due to wall friction is approximated by pipe data. Most analyses use information obtained with centrifugal pumps and compressor volutes, or it is frequently stated in the literature that designers must account for these effects by experience. A nearly circular cross section is desirable since it passes the largest volume flow rate per surface area, thereby minimizing wall friction losses. In radial turbines nearly-circular scroll cross sections can be used in conjunction with inlet guide vanes since the flow is accelerating and can pass smoothly from the manifold to the guide vanes.

The existing area distribution of the scroll is shown in Fig. 17. There is nearly a linear decrease in area with angle of advance. Eckert [13] gives a relation that establishes the required flow area as a function of angular position for a compressor volute. This relation, although approximate, includes the effect of increased average velocity with decreased mean radius for circular cross sections. A second relation can be used to correct the determined areas for frictional losses. The relations can be applied to the turbine scroll if the terms are defined in an appropriate manner. An area distribution calculation is carried out in Appendix B and the results are shown in Fig. 17. The area distribution resulting from the calculation is very close to that of the existing scroll.

In order to determine the pressure distribution in the present inlet manifold and to evaluate its performance, eleven static pressure taps were installed around the outer periphery. The positions of these taps, which were placed at 30 degree intervals near the bisecting plane of the scroll, are shown in Fig. 2. Eight static pressure taps were already installed on either side of the scroll ahead of the inlet guide vanes. The positions of these taps are shown in Fig. 2 and 6. The pressures obtained by these static taps were measured on the 96-inch water manometer board for all test runs.

Fig. 18 and 19 show the pressure distributions around the outer periphery of the scroll, and ahead of the inlet guide vanes, at a pressure ratio $\frac{P_{to}}{P_{atm}} = 1.449$. This ratio corresponds to a mass flow rate $W_{vc} = 1.875$ lbm/sec which is near to that of the design point for the model turbine tests. These data were taken while performing a dummy rotor torque test and the pressure distribution is qualitatively representative of that observed for all tests with the dummy rotor. However the distribution was different if the dummy rotor was removed, indicating that the flow before the guide vanes was influenced by the aforementioned unusual conditions downstream of the guide vanes. With the dummy rotor removed it was observed that static pressures on the periphery were reduced at taps 6 and 7, and increased at taps 9 and 10, relative to those with the dummy rotor installed. The static pressure generally decreases around the outer periphery of the scroll. This may be due to the decreasing outer radius of the scroll with angle of advance which increases the velocity there if angular momentum is conserved. The static pressure level around the outer periphery is nearly equal to that at the inlet. The static pressure before the guide vanes around the circumference increases considerably with the angle of advance and is lower than the inlet pressure at all stations. Particularly low pressures existed at taps 1 and 2 near the inlet and at taps 8 (right and left) in the tongue of the scroll. These relatively low pressures may result from flow accelerations caused by the radial inlet pipe. The radial inlet pipe was a requirement in the original model test simulating the actual machine. It provided structural integrity for very high pressure operation. With interest directed toward performance improvement as well as performance evaluation and prediction, it would be preferable to have a tangential inlet. Conditions might also be improved by increasing the radius of curvature and/or installing a turning vane at the inlet to the scroll. The pressures measured at taps 8 (right and left) in the tongue may be influenced by the relative position of the nearest guide vane. The pressure distribution may in fact be affected by the guide vane positions, since there are seven guide vanes but eight static taps on each side. The influence of guide vane position on the pressure distribution should be checked before changes are made to the scroll area distribution. Because the pressure distribution was dependent on the configuration after the guide vanes, it would be advisable to determine the pressure distribution during turbine tests. The scroll casing has been equipped to accept total pressure probes at three of the static tap positions around the periphery.

Total pressure measurements at these stations would provide more information about the losses and the velocity distribution in the scroll. The "dynamic" pressure distribution shown in Fig. 19 is necessarily based on conditions at the scroll inlet. Measurements indicate that improvement of the pressure distribution before the guide vanes could be accomplished by increasing the cross-sectional area of the scroll in decreasing proportions with angle of advance.

6. Vortex Chamber Flow

Installation

To obtain a better understanding of the conditions existing in the vaneless space after the inlet guide vanes, the turbine test rig was modified to carry out special tests. The existing plexiglas turbine shrouds, with contours that follow the turbine rotor profile, were replaced by flat, parallel-faced plexiglas plates which extended inward axially so that their inside faces were in the same plane as the rings supporting the inlet guide vanes. This in effect provided a flat vortex chamber in which air would be injected nearly tangentially across the width through the existing guide vanes. A cross section of this installation is shown in Fig. 20. The right-hand side plate of the vortex chamber contains an aluminum orifice plate which is recessed so that the inner face is flush with the inner face of the plexiglas plate. The orifice plate can be replaced by other plates with different orifice diameters. The plate for the present tests has a 2.50 inch orifice diameter. The so-called left-hand side plate of the vortex chamber was machined so that it could be fitted with a four-inch inside diameter aluminum pipe which would serve as a vortex tube for future experiments. This tube shown in Fig. 20 was not installed for the main part of this investigation.

The outer diameters of the abovementioned plexiglas plates of the vortex chamber are 9.50 inches, leaving a small annulus around their periphery in which the static pressure after the guide vanes can be measured relatively free from the local influences and/or wakes of the guide vanes. Static pressure taps were also placed at different radii on the inner surfaces of the plates along a logarithmic spiral from the outer radius to the discharge radius. The logarithmic spiral represents the path of a gas particle in an incompressible, frictionless flow based on an injection angle α_i = 79.2 degrees at the radius R_i = 4.75 inches. Initial tests were conducted with a coating of carbon-black and kerosene on the vortex chamber side plates. The observed streamlines, on the walls as shown by the carbon-black, deviate considerably from a theoretical logarithmic spiral. The carbon-black traces show that the direction of the flow particles close to the wall have considerably reduced flow angles. This can be due to either increased radial velocity components, or decreased tangential velocity components where the latter effect is more probable. Static pressure taps were also placed at different radii along a streamline obtained from the carbon-black traces. The difference of the pressures measured were very small at the same radii along the two curves. Hence it was decided to use only the taps along the theoretical logarithmic spiral on each chamber side plate for the subsequent tests. The static pressures could be measured with an accuracy of $\pm$ 0.05 inch on the 96-inch manometer board.

A United Sensor DA-125 three-dimensional pressure probe was used to determine the flow angles and pressures across the axial width of the vortex chamber at radii of 3.00 and 4.50 inches. The DA-125 probe is similar to the SA-120 probe described in section 4 but it is shorter.

The total temperature was also surveyed with the probe described in section 4 across the axial width of the vortex chamber but only at a radius of 3.00 inches. At each axial position the temperature probe was set at the same yaw angle determined by the DA-125 pressure probe. The test installation for the vortex chamber surveys is shown in Fig. 21 and 22.

Testing and Results

To determine whether flow nonuniformities occur around the periphery of the vortex chamber after the guide vanes the pressure probe was installed at the center plane at a radius of 3.00 inches. With the probe exactly lined up with the prevailing flow directions the entire chamber end was rotated slowly while the dynamic pressure head was observed on the manometer board. Since no changes in this pressure could be observed it can be assumed that the guide vane wakes are equalized at this radius. The aforementioned procedure was also carried out at a radius of 4.50 inches. It was noticed that the dynamic head decreased about one or two percent as the probe passed through the guide vane wakes as verified by their angular separation. In these wakes the flow also became slightly more tangential. Flow angle surveys are shown in Fig. 23 for peripheral positions which can be considered to be inside and outside of the wake.

The wake position that was noticed at a radius of 4.50 inches was about 54 degrees away from the circumferential position of the guide vane trailing edge. Maximum dynamic pressure seemed to occur at a position of about 26 degrees from the wake. This position coincides with a mean streamline between guide vanes since relative positions in the guide vane flow are separated by about 51.5 degrees ($360^{\circ}/7$).

Fig. 23 shows that the flow angle distribution changes considerably with decreasing radius. At the 3.00 inch radius the flow angle near the center plane has increased to 90 degrees, while at the side walls the flow angle has decreased considerably from that at a radius of 4.5 inches. This increase in radial velocity components near the side walls was observed from carbon-black and kerosene test. A photograph of the vortex chamber side walls after the carbon-black and kerosene test is shown in Fig. 24.

The dynamic pressure distribution shown in Fig. 25 is nearly uniform over the axial width of the chamber but decreases at the side walls. The dynamic pressure at a radius of 3.00 inches is approximately double that at the radius of 4.5 inches.

The survey at a radius of 3.00 inches at a pressure ratio $\frac{P_{to}}{P_{atm}} = 1.242$ indicated that the total pressure near the center plane of the vortex chamber was greater than that at the manifold inlet. To assure that this result was factual the pressures were measured relative to each other on the U-tube water manometer. In the 4.50 inch radius surveys the total pressure recovered in the vortex chamber was near to but not greater than the total pressure at the manifold inlet. The total pressure distribution is shown in Fig. 26.

The three-dimensional pressure probe can produce measurement errors when introduced into small passages or when used near walls. Although the vortex chamber width is small (0.784 inch), the blockage effect, that can falsify static pressure readings, will be small since the flow area is the meridional cross section at the survey radius. Pitch angle and static pressure measurement may be in error near walls due to the effects of secondary flow along the probe shaft since the probe calibrations hold for deep immersion only. The pitch angles and the static pressures which are obtained from the calibration curves may therefore be inaccurate. Very near the wall the pitch angle determination is unreliable because one of the pressure sensing taps will be inside the access hole but yaw and total pressure data will still be accurate because these data do not require the use of calibration curves.

In traversing the axial width of the vortex chamber with the pressure probe it was observed that the pitch angle changed from negative near the so-called left-hand wall to positive near the so-called right-hand wall. This indicated that the flow was turned toward the wall on either side of the center plane. Although this may be due to wall effects on pitch angle determination it is more than likely that this flow pattern is an indication of the existence of axial flow components toward the side walls and the presence of secondary flow vortices.

The temperature survey was first conducted with the inlet air at an average temperature of 121.5°F at pressure ratios of $\frac{P_{to}}{P_{atm}} = 1.236$ and 1.484. The results of these surveys are shown in Fig. 27. A symmetrical total temperature profile existed in both runs with the highest temperatures recorded near the center plane of the chamber. The higher pressure and mass flow rate produced a larger temperature gradient across the width of the chamber. The total temperatures in the vortex chamber were below the inlet temperature at all axial positions. The inlet air temperature was considerably higher than the ambient temperature, hence temperature drops did occur because of heat transfer from the test apparatus to the surroundings. This is evidenced by the drop in total temperature of about 7°F from the flow measuring orifice to the manifold inlet ahead of the vortex chamber.

Another test was then made with conditions to produce nearly adiabatic conditions. The supply air was cooled as much as possible and the temperature recorded at the flow-measuring orifice was only about 2°F higher than the ambient temperature in the test cell. The Kiel temperature probe at the manifold inlet was replaced by one which is identical to that used for the survey in the vortex chamber to avoid measuring inaccuracies. Before installing this probe its output was compared in still air with the one used for the survey and no difference could be observed. Surveys were then made at a radius of 3.00 inches at pressure ratios of $\frac{P_{to}}{P_{atm}} = 1.236$ and 1.484. Since the inlet temperature was increasing slightly during the test time, the difference between the temperature recovered at axial positions in the vortex chamber and the total temperature at the inlet is shown in Fig. 28. A symmetrical axial temperature profile was obtained again but the temperature difference is positive near the center and negative near the side walls. Since it can be assumed that the instrumentation is reliable, it appears that the total temperature recovered near the center plane of the vortex chamber is higher than that at the inlet. The possibility of heat being transfered from the surroundings to the flow must be ruled out since the contact areas where high velocities exist are small. It seems feasible therefore that energy separation is taking place in the flow and that the flow at the side walls gives up energy to that in the center. This result supports the measured fact of a higher total pressure near the center plane of the vortex chamber than at the manifold inlet, even with an increase in entropy due to frictional effects.

Limited testing was conducted with a 42-inch by four-inch inside diameter vortex tube attached to the left end of the vortex chamber. A conical valve was inserted in the tube end to divide the flow discharge between the annulus, thus formed, and the orifice on the opposite end. Total temperature separations of nearly 30°F were sensed at a pressure ratio $\frac{P_{to}}{P_{atm}} = 1.5$. Instrumentation was employed to to demonstrate the effect in an approximate manner; however, the installation could readily accept instrumentation with very little disturbance to the flow because of its size and the large flow capacity of the facility.

Ranque-Hilsch Effect

Many studies have been conducted on the behavior of vortex flow in cylinders. Much of this interest was concerned with the Ranque-Hilsch tube. In such a device compressed gas is injected tangentially at the circumference near one end of a tube. This results in a vortex core near the axis which is at a lower total temperature than that of the inlet gas, whereas the gas in the annulus surrounding the core is at higher total temperature. Different configurations have been utilized to separate the hot and cold flows. Usually the cold stream is extracted through an orifice on the injection end while the hot stream discharges from an annular region at a larger radius on the opposite end of the tube. However, a counterflow configuration such as this is not essential in producing the separation. The process is referred to as the Ranque-Hilsch effect, total temperature separation, or energy separation. Harnett and Eckert [9] in experiments they conducted with a vortex tube found that the greatest energy separation took place in the tube cross section near the tangential nozzles. Work by Savino and Ragsdale [10] indicates that considerable energy separation can take place in a vortex contained between two flat plates without an attached tube. In their experiment, the flow emerged from an opening at the center with a diameter on the order of the plate spacing; and most of the energy separation took place near the opening. In the present investigation higher total temperatures and pressures than those at the inlet were found to occur at the smaller survey radius of 3.00 inches.

Deissler and Perlmutter [11] concluded from an analytical investigation that the most important factor affecting the total temperature of a fluid element in a compressible vortex is the turbulent shear work done on or by the element. Although no conclusive evidence exists as to the exact mechanism causing energy separation, there seems to be general agreement that it is brought about by the so-called turbulent or eddy viscosity. A parameter on which energy separation seems to be dependent is a turbulent radial flow Reynolds number which is expressed either with the eddy viscosity only, or together with the molecular viscosity. The turbulence of the flow causes the effective Reynolds number to remain low even when the Reynolds number based on molecular viscosity is high. This occurs because the turbulent viscosity may be several orders of magnitude higher than the molecular viscosity. In some analyses the molecular viscosity is neglected. It appears, however, that there is an optimum turbulence for separation since diffusion will counteract the separation caused by increased viscosity if turbulence is increased indefinitely.

It appears also that energy separation depends on the deviation of the tangential velocity profile from that for an inviscid flow. Since a free vortex flow requires the impossible condition of infinite velocity at the axis, such deviations will always occur in flows of real fluids. In section 4 the survey of the turbine rotor discharge section, with the rotor removed, showed that the velocity decreases with decreasing radius. The velocity profile is more nearly that of a forced vortex or rotating solid than the one which would occur in a free vortex flow. The discharge flow of the vortex chamber was not surveyed but results of the axial traverse at a radius of 3.00 inches indicate that the flow near the mid-plane deviates considerably from inviscid flow since there was no radial velocity component. Some investigators feel that temperature separation will only appear in regions where an axial variation of the mass flow can be established such as would occur near the discharge area.

Vortex Chamber One-Dimensional Analysis

The flow in a vortex chamber with parallel side walls perpendicular to the axis of symmetry can be considered to be axisymmetric. If the flow is uniformly injected at the radius R_i with a known Mach number M_i and flow angle α_i, a one-dimensional analysis can be made to determine the Mach number M and flow angle α, at an arbitrary radius R less than R_i. Such an analysis has been carried out by Vavra [12]. The flow is considered to be compressible and steady. It is assumed that frictional losses are negligible and the process is adiabatic. The analysis assumes no velocity components or velocity gradients in the axial direction. If the width of the chamber is b, continuity is satisfied at an arbitrary radius R by

$$\rho 2\pi R b V_m = \rho_i 2\pi R_i b V_{mi}$$

or since $V_m = V\cos\alpha$ and $V_{mi} = V_i \cos\alpha_i$

$$\rho R V \cos\alpha = \rho_i R_i V_i \cos\alpha_i$$

By introducing the acoustic velocities, there is

$$\rho R M \cos\alpha = \rho_i R_i M_i \cos\alpha_i \left(\frac{a_i}{a}\right) \tag{6-1}$$

With the flow being frictionless, no moment is exerted by the walls on the flow, and angular momentum is conserved. Then at an arbitrary radius R

$$R V_u = R_i V_{ui}$$

with

$$V_u = V\sin\alpha \quad \text{and} \quad V_{ui} = V\sin\alpha_i$$

there are

$$R V \sin\alpha = R_i V_i \sin\alpha_i$$

and

$$R M \sin\alpha = R_i M_i \sin\alpha_i \left(\frac{a_i}{a}\right) \tag{6-2}$$

From equations (6-1) and (6-2)

$$\tan\alpha = \tan\alpha_i \left(\frac{\rho}{\rho_i}\right) \tag{6-3}$$

Since the flow is assumed to be adiabatic, total energy is conserved and

$$c_p T + \frac{V^2}{2gJ} = c_p T_i + \frac{V_i^{\,2}}{2gJ}$$

With

$$c_p = R_g \frac{\gamma}{\gamma - 1}$$

and the acoustic velocities,

$$1 + \frac{\gamma-1}{2} M^2 = \frac{a_i^2}{a^2}\left(1 + \frac{\gamma-1}{2} M_i^2\right) \tag{6-4}$$

Since the flow is assumed to be isentropic

$$\frac{a_i^2}{a^2} = \frac{T_i}{T} = \left(\frac{\rho_i}{\rho}\right)^{\gamma-1} = \left(\frac{p_i}{p}\right)^{\frac{\gamma-1}{\gamma}}$$

Then, with pressure ratio, p/p_i

$$M = \left\{\frac{2}{\gamma-1}\left[\left(\frac{p_i}{p}\right)^{\frac{\gamma-1}{\gamma}}\left(1 + \frac{\gamma-1}{2} M_i^2\right) - 1\right]\right\}^{\frac{1}{2}} \tag{6-5}$$

and

$$\tan\alpha = \tan\alpha_i \left(\frac{p}{p_i}\right)^{\frac{1}{\gamma}} \tag{6-6}$$

Mach number M and flow angle α are then known as a function of inlet conditions and pressure ratio. The radius can be determined from equation (6-2) by replacing the ratio of the acoustic velocities by the pressure ratio, giving

$$R = R_i \frac{M_i \sin\alpha_i}{M \sin\alpha}\left(\frac{p_i}{p}\right)^{\frac{\gamma-1}{2\gamma}} \tag{6-7}$$

To apply this analysis to the results obtained in tests it is necessary to know M_i and α_i at some radius R_i in the vortex chamber. Pressures and temperatures were not available in the same test run, hence the Mach number M_i is unknown. By extrapolating data from the dummy rotor torque tests there are $M_i = .175$ and $\alpha_i = 79.2^\circ$ at $R_i = 4.75$ inches, at $\frac{P_{to}}{P_1} = \frac{P_{to}}{P_i} = 1.024$. The theoretical pressure distribution obtained with these conditions is shown with a broken curve in Fig. 29. Although the form of the curve compares well with the actual static pressure distribution it does not coincide with it. However, since the theoretical pressure distribution depends greatly on the value of M_i an exact comparison is difficult.

Fig. 30 shows the results of the theoretical analysis for $M_i = 0.175$. It is of interest to note that supersonic flow could be obtained without converging-diverging flow areas at a radius ratio R/R_i less than about 18% but the flow does not choke until a ratio of R/R_i of about 15% is reached. Choking can occur only if the Mach number of the radial velocity component is unity whereas the Mach number of the actual velocity is greater than unity. An oblique or normal shock can occur in the flow only if the component of velocity normal to the shock is supersonic. From consideration of the axial symmetry of the flow in the vortex chamber, this would require that the shock be a circular cylinder. Then the flow could not be choked with a subsonic radial velocity component even though the velocity is supersonic because there are large peripheral components.

These interesting aspects of the vortex chamber have not been realized in the subject investigation. To acquire survey data and to remain within the capability of the instrumentation as it was initially installed, the maximum pressure ratio at which tests were made was $\frac{P_{to}}{P_{atm}} = 1.553$. This is well below that which would theoretically produce supersonic flow; however, it appears from an extension of the test data that the required theoretical pressure ratio is within the capability of the compressor. Also since the flow becomes supersonic at a larger radius ratio if the injection Mach number is higher, the existing vortex chamber geometry may meet the requirements.

The influence of viscosity in the vortex chamber flow, however, could prevent supersonic flow conditions. The flow paths, especially near the center plane of the chamber, are long, and viscous effects dominate. That these effects are large has been demonstrated by the departure of the flow angle of the real flow from the theoretical one. The increased radial velocity components near the side walls must result from wall friction but it appears that they may be initiated by secondary flow in the curved channels between the inlet guide vanes before the flow enters the chamber.

The considerable change in flow angle across the axial width of the vortex chamber is of interest to the turbine designer. Within the limitations imposed by structural and manufacturing requirements the rotor tip could be designed to accept the flow as it actually exists and it seems possible to reduce the losses with such a procedure.

The flow in a vortex chamber with the geometry investigated is truly three-dimensional. The flow develops quickly and there appears little possibility of separating a "boundary layer" on the side walls from a potential flow near the center plane. Even in a chamber of this geometry, where the axial width is small compared to the diameter, there appears to be evidence of axial velocity components which should be considered in an analysis. Knowledge about turbulent flows and turbulent boundary layers in general is limited. Laws predicting separation for even two-dimensional boundary layer flows are inadequate. In the vortex chamber the flow is complicated by the existence of a pressure gradient and the three-dimensional aspects, including the fact that there is more than one large velocity component. Complete analysis of the flow is a problem of great magnitude.

Fig. 1. Wooden Scroll Insert

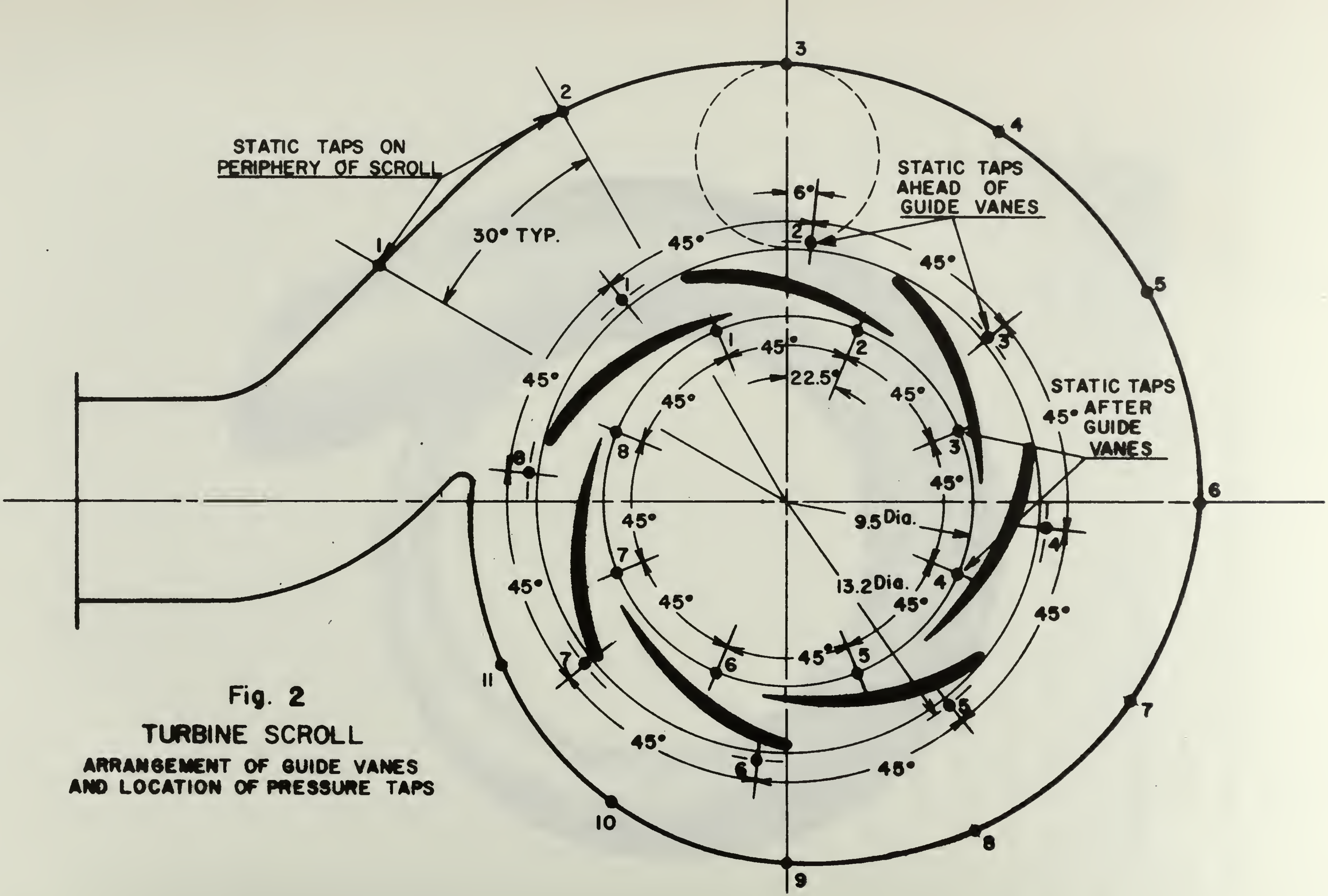

Fig. 2

TURBINE SCROLL

ARRANGEMENT OF GUIDE VANES
AND LOCATION OF PRESSURE TAPS

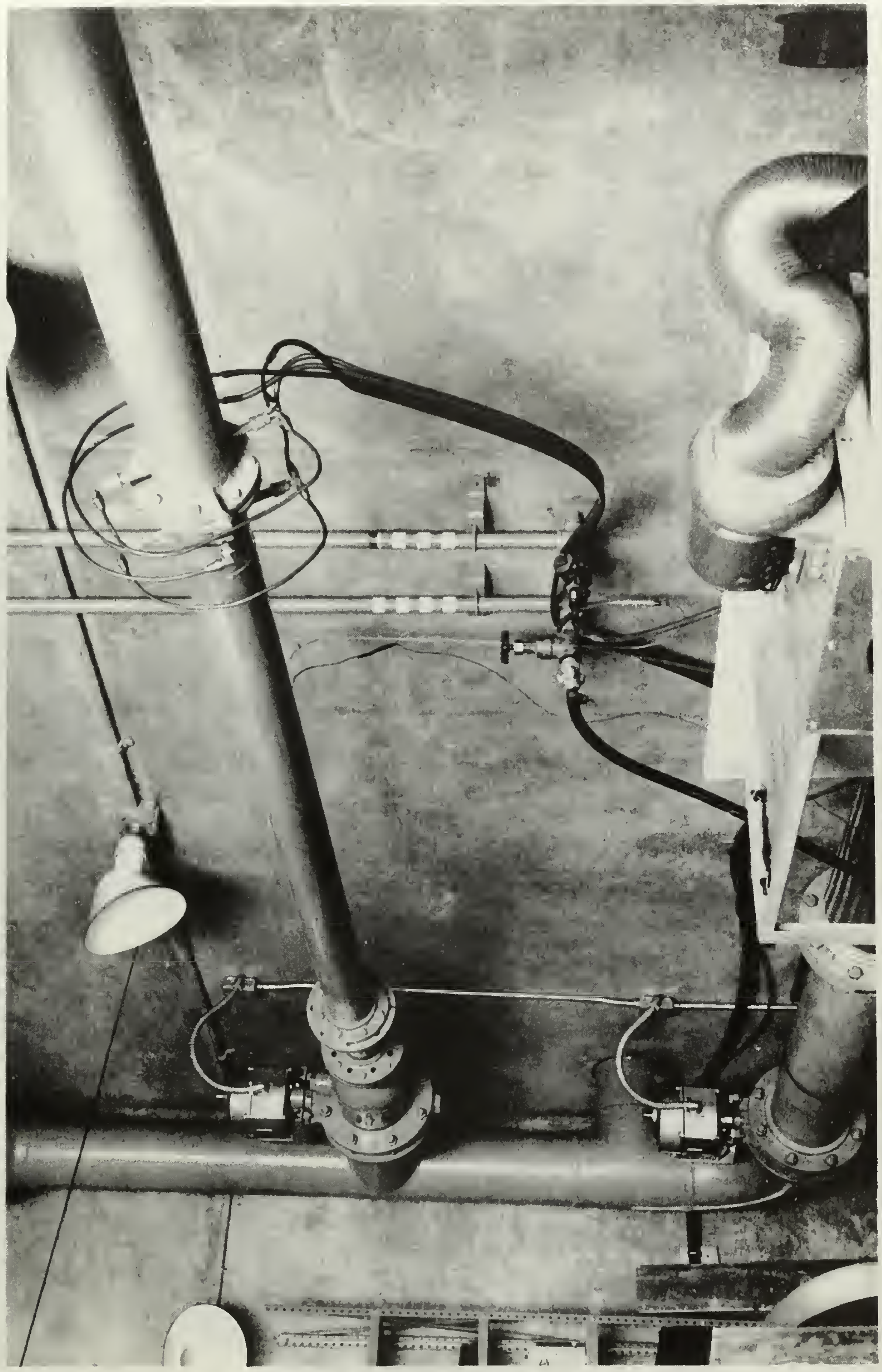

Fig. 3 Four-inch Pipe with Remote Controlled Valve and Flow-measuring Orifice

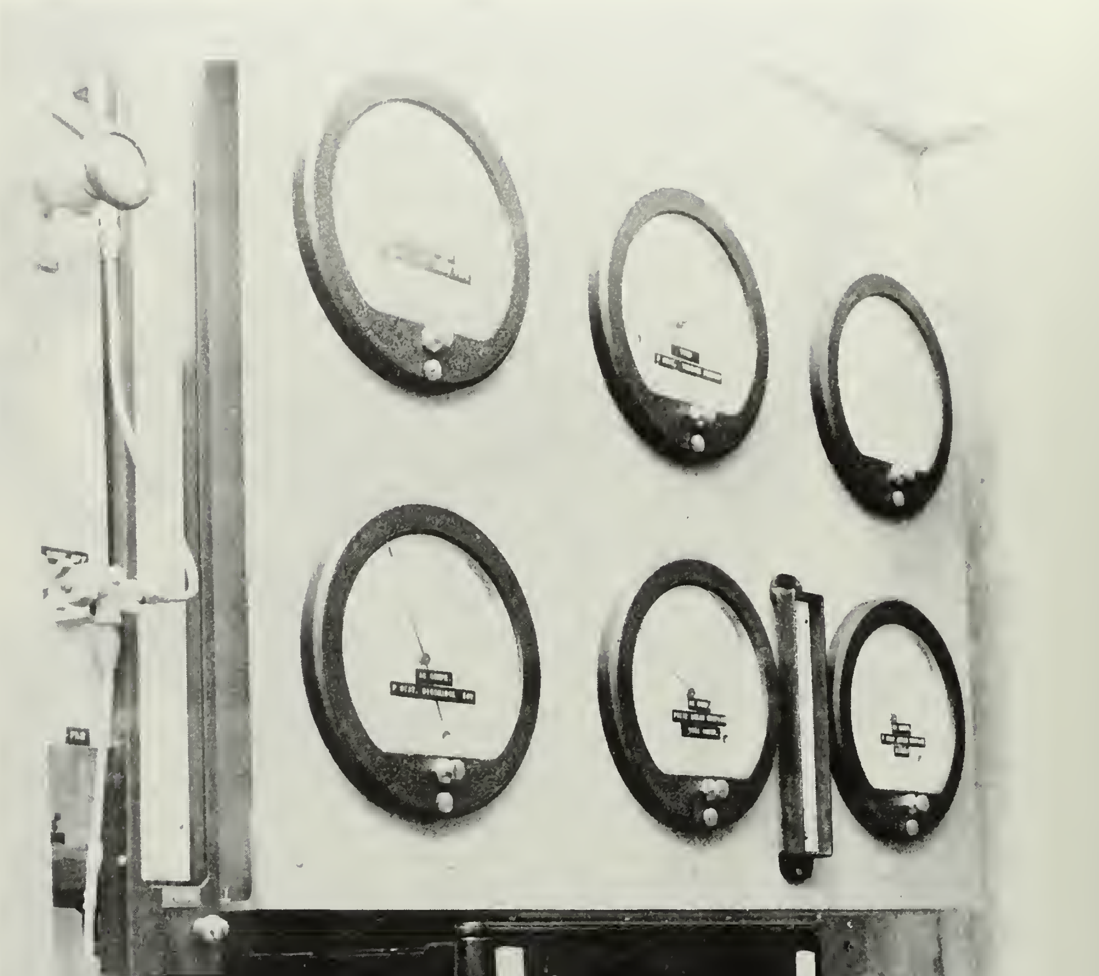

Fig. 4 Heise Gage and Brown Potentiometer

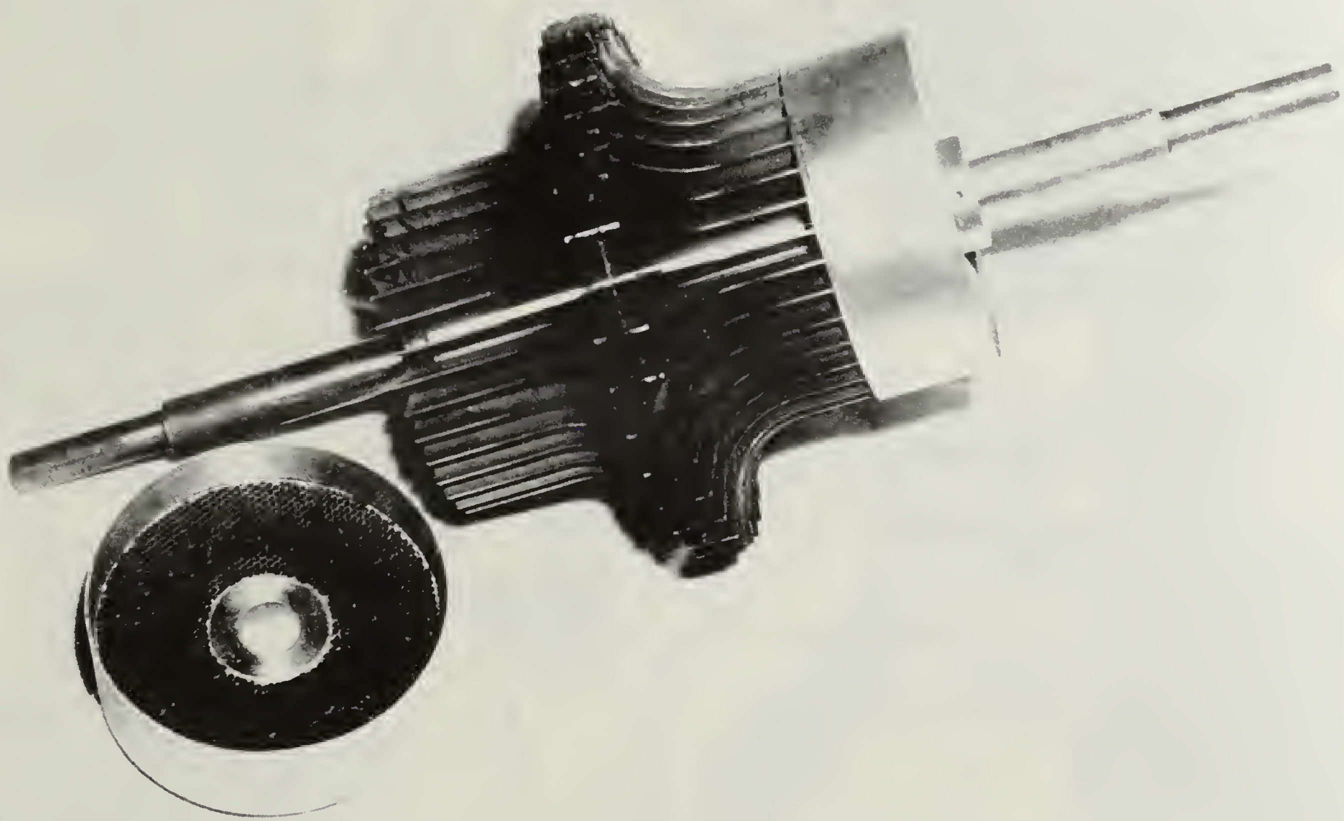

Fig. 5 Dummy Rotor with Honeycomb Flow Straighteners

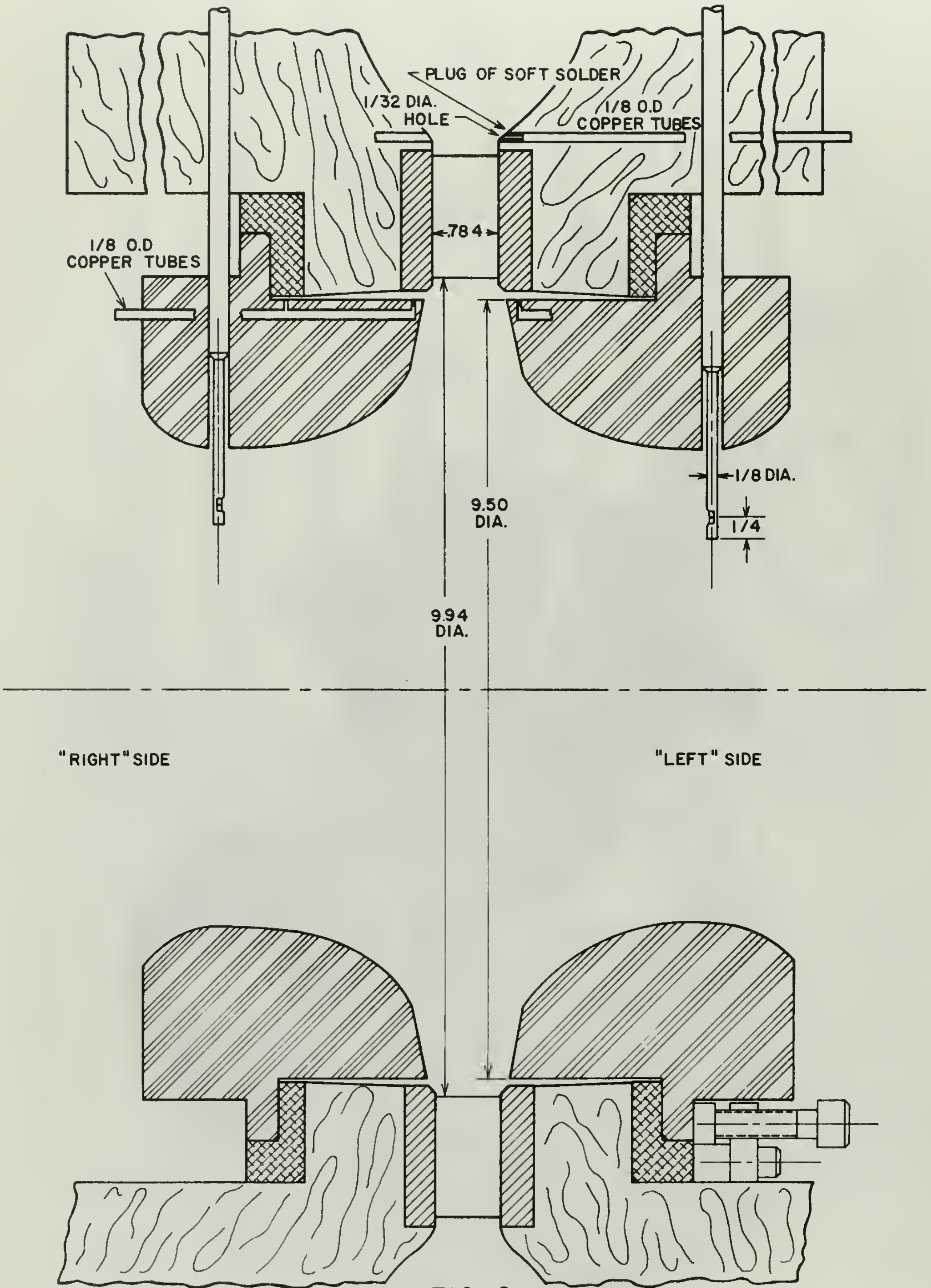

FIG. 6
CROSS SECTION OF TURBINE WITHOUT ROTOR

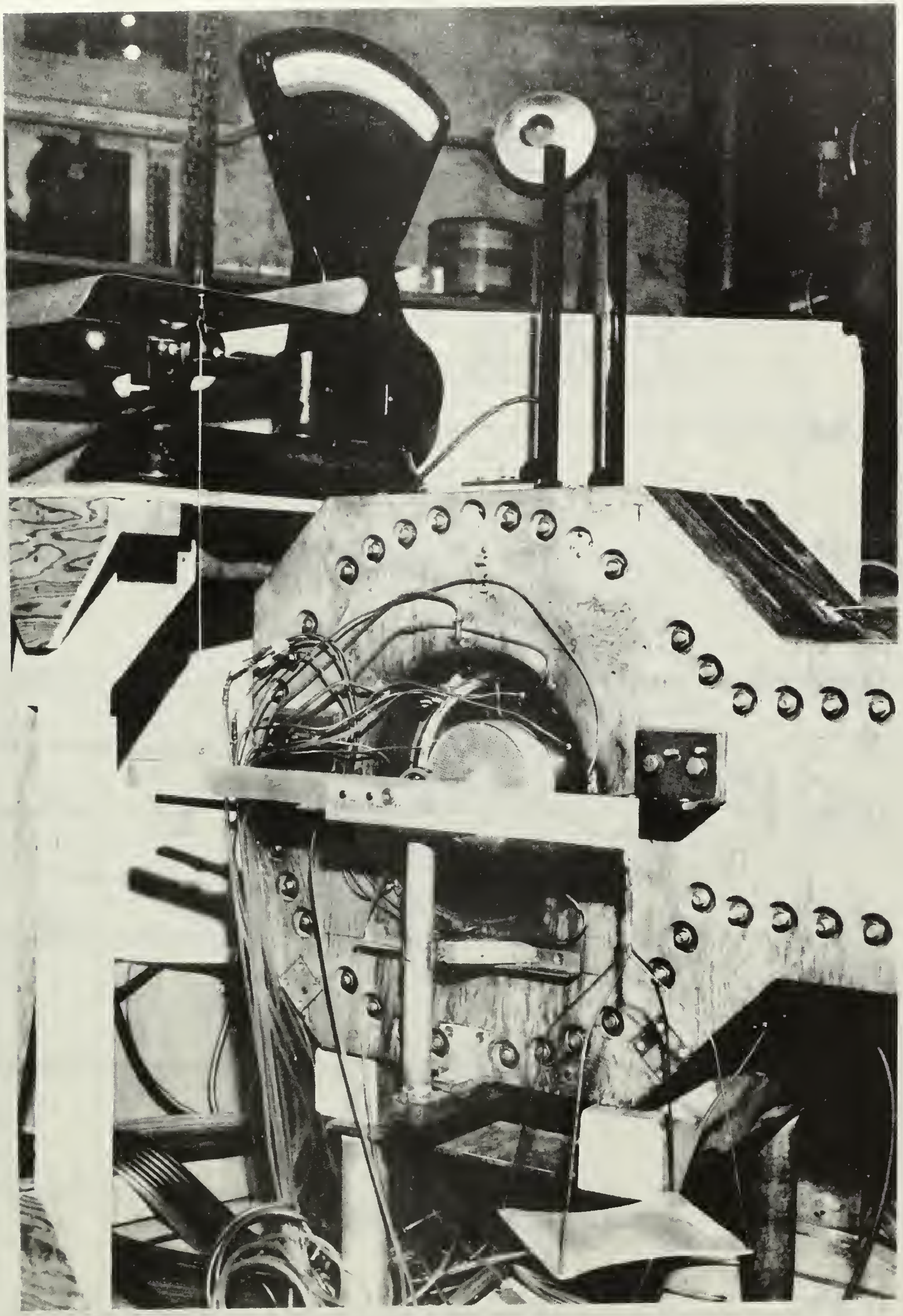

Fig. 7 Dummy Rotor Test Installation

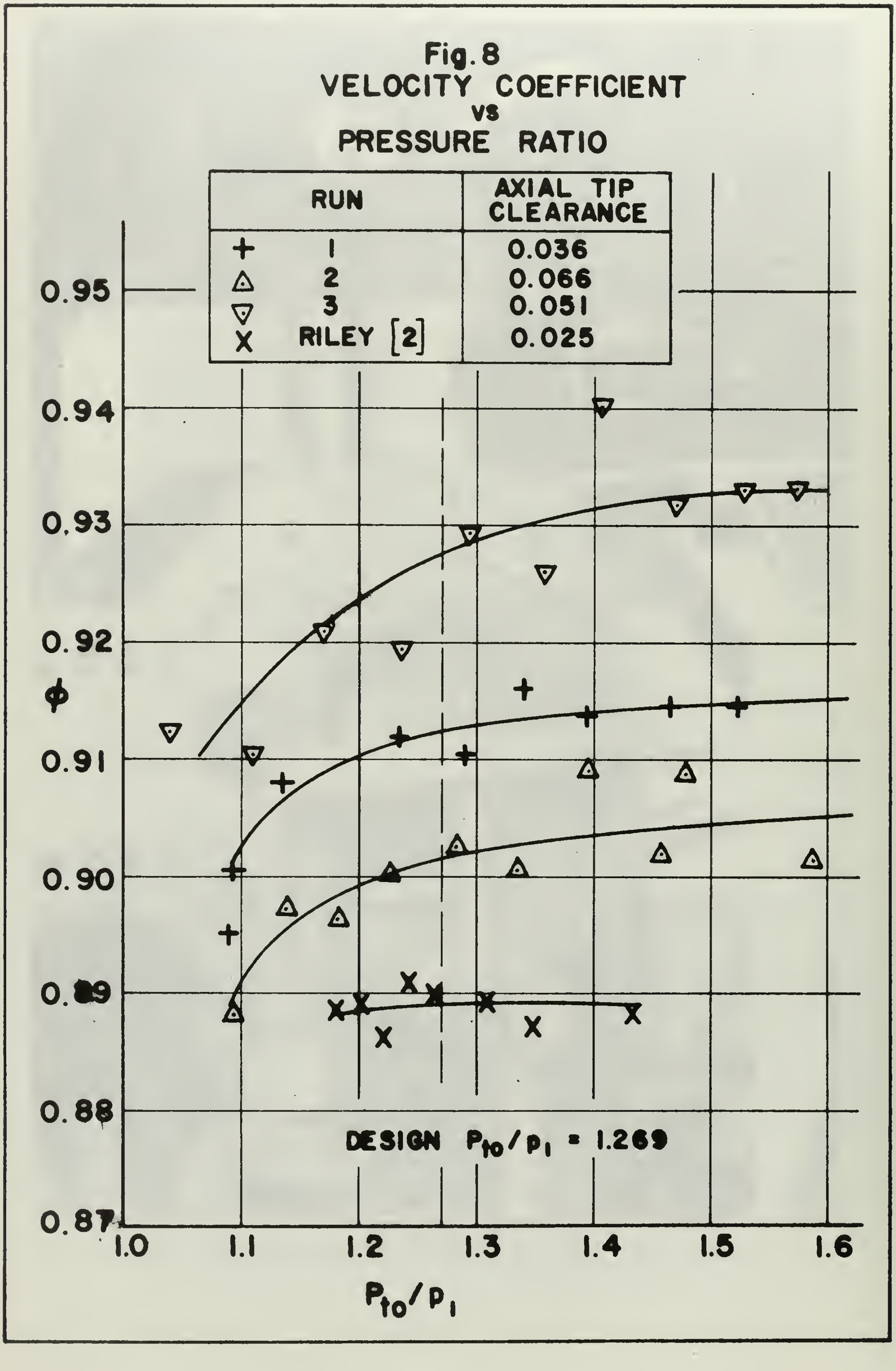
Fig. 8
VELOCITY COEFFICIENT
vs
PRESSURE RATIO
RUN | AXIAL TIP CLEARANCE
+ 1 0.036
△ 2 0.066
▽ 3 0.051
X RILEY [2] 0.025
0.95
0.94
0.93
0.92
φ
0.91
0.90
0.89
0.88
0.87
1.0
1.1
1.2
1.3
1.4
1.5
1.6
DESIGN P_{t0}/p_1 = 1.269
P_{t0}/p_1

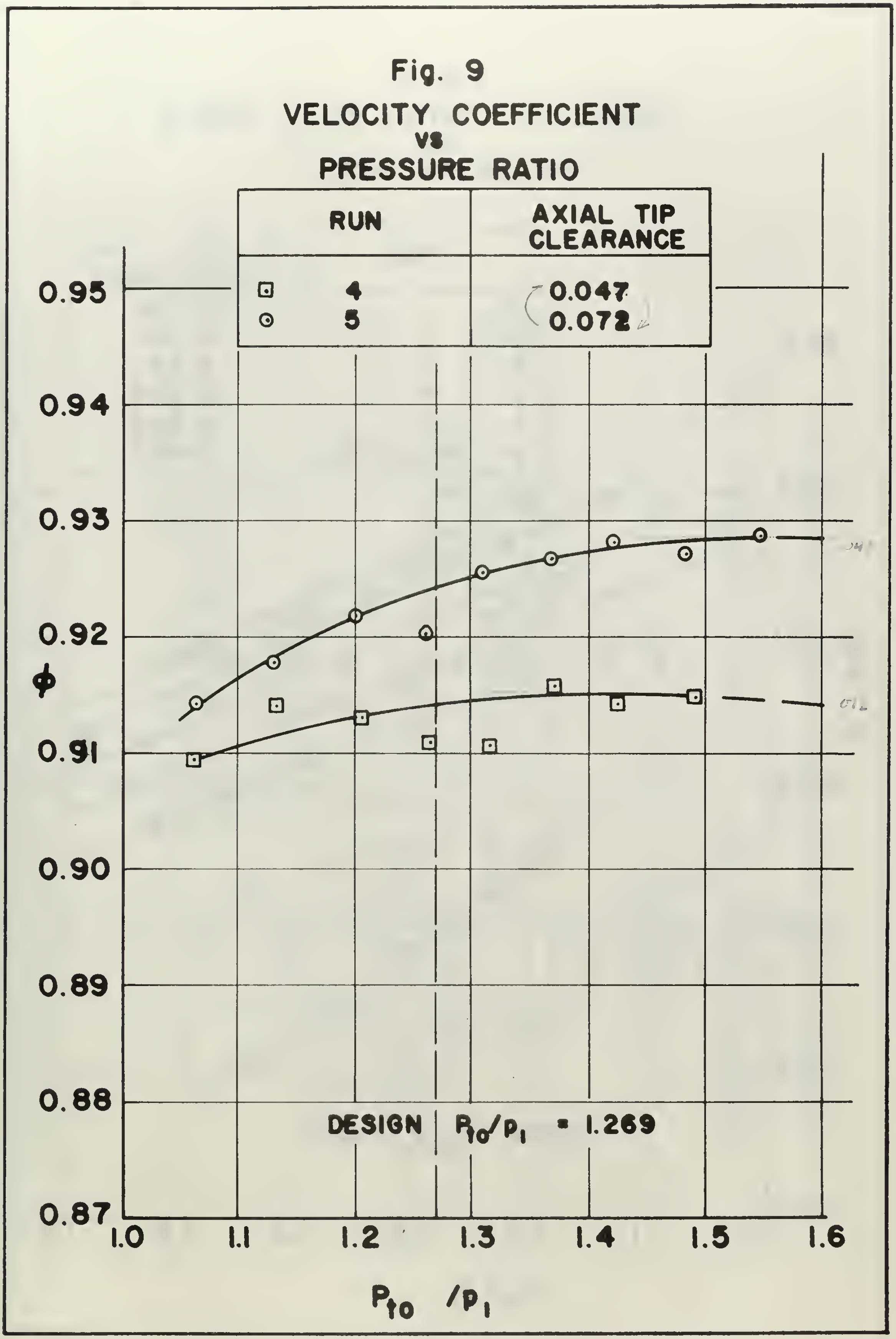
Fig. 9
VELOCITY COEFFICIENT
vs
PRESSURE RATIO
RUN
AXIAL TIP CLEARANCE
4
0.047
5
0.072
0.95
0.94
0.93
0.92
0.91
0.90
0.89
0.88
0.87
φ
DESIGN P_{t0}/p_1 = 1.269
1.0
1.1
1.2
1.3
1.4
1.5
1.6
P_{t0}/p_1

Fig. 10
ABSOLUTE ROTOR INLET ANGLE
vs.
PRESSURE RATIO

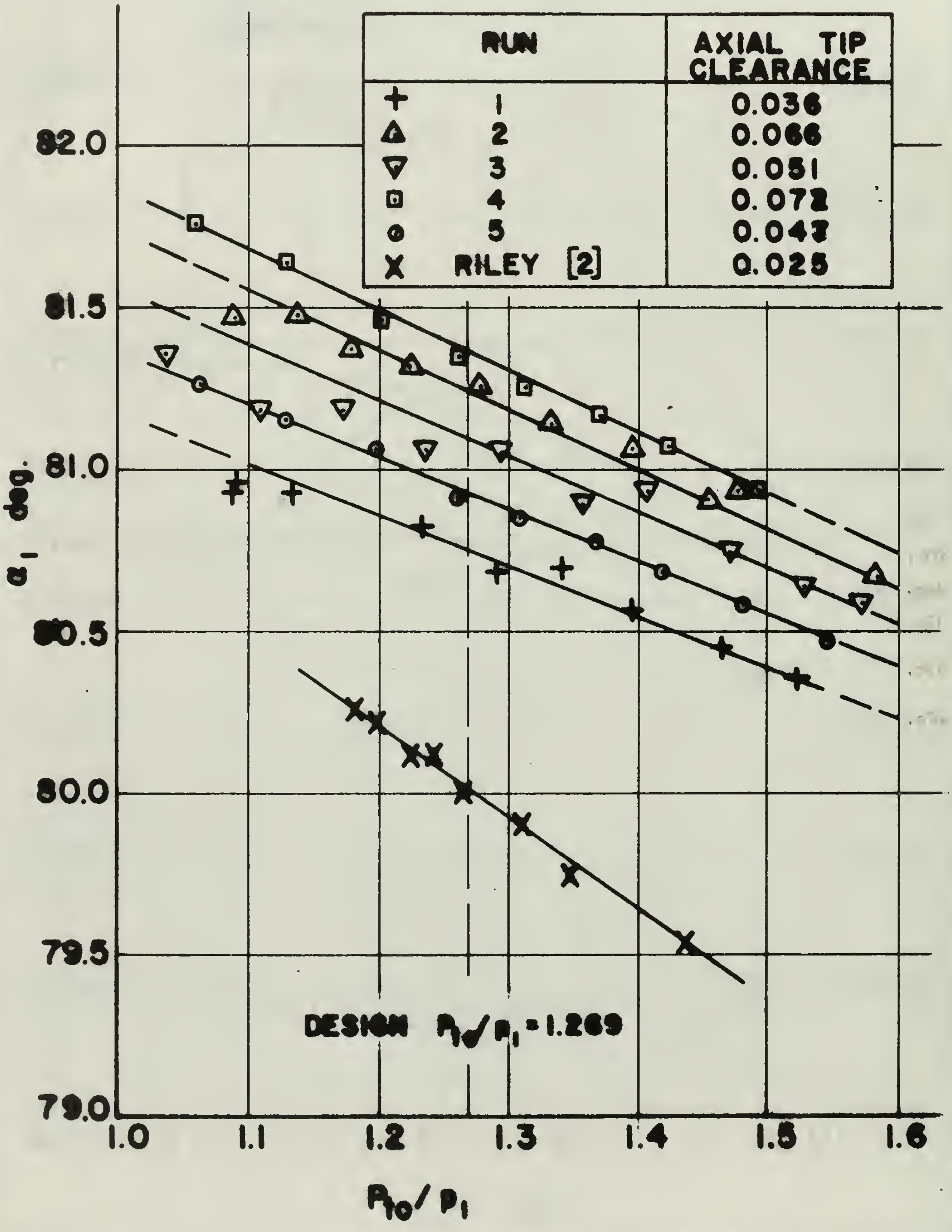

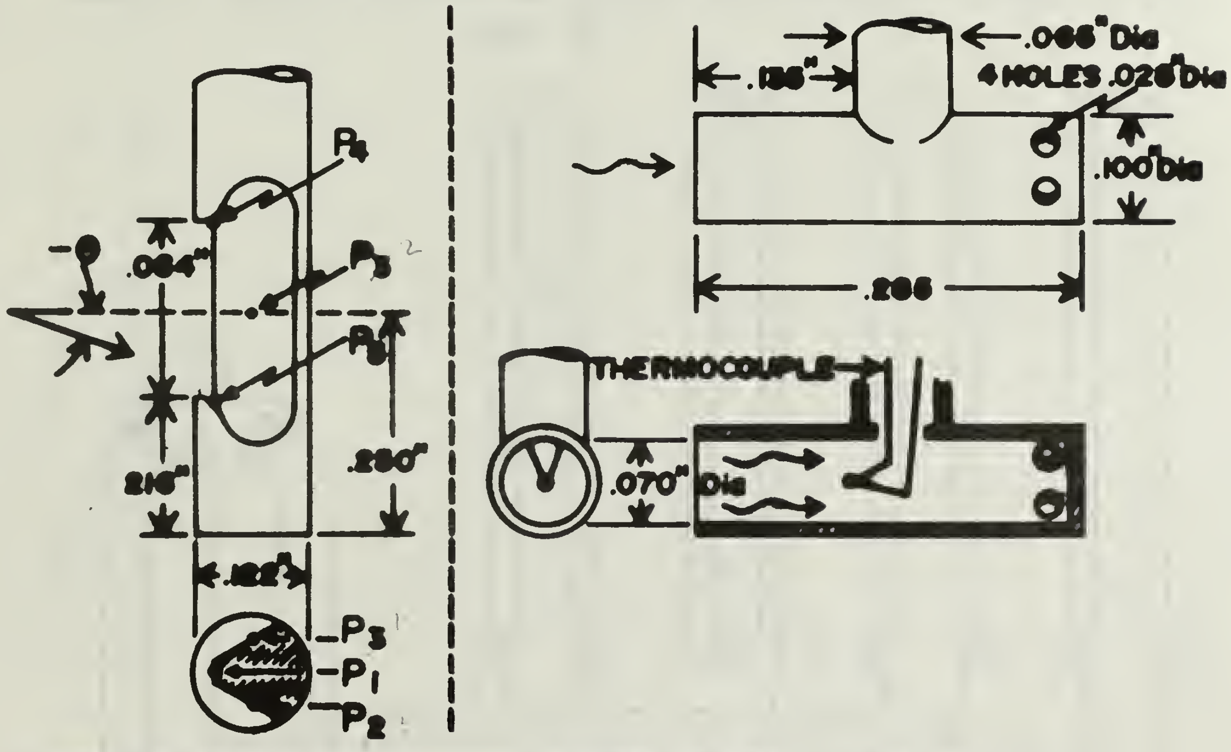

PRESSURE PROBE HEAD TEMPERATURE PROBE HEAD

FIG. 11

PRESSURE AND TEMPERATURE SURVEY PROBE HEADS

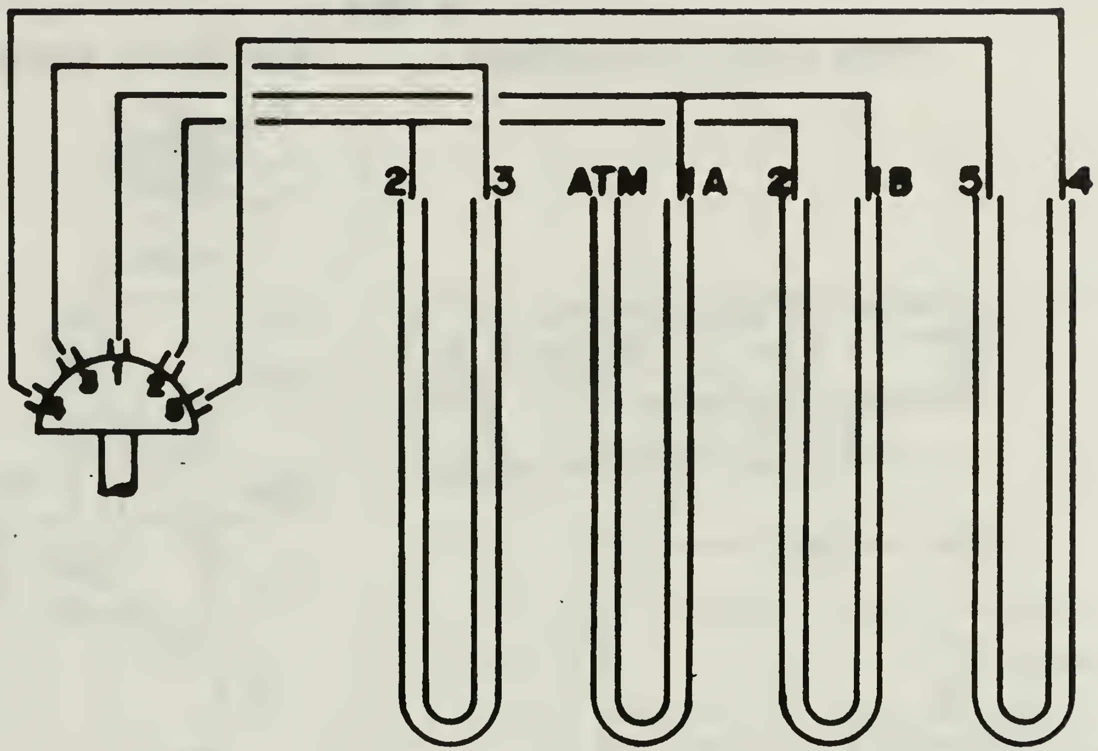

FIG. 12
TYPICAL DA-120 PRESSURE PROBE MANOMETER CONNECTION

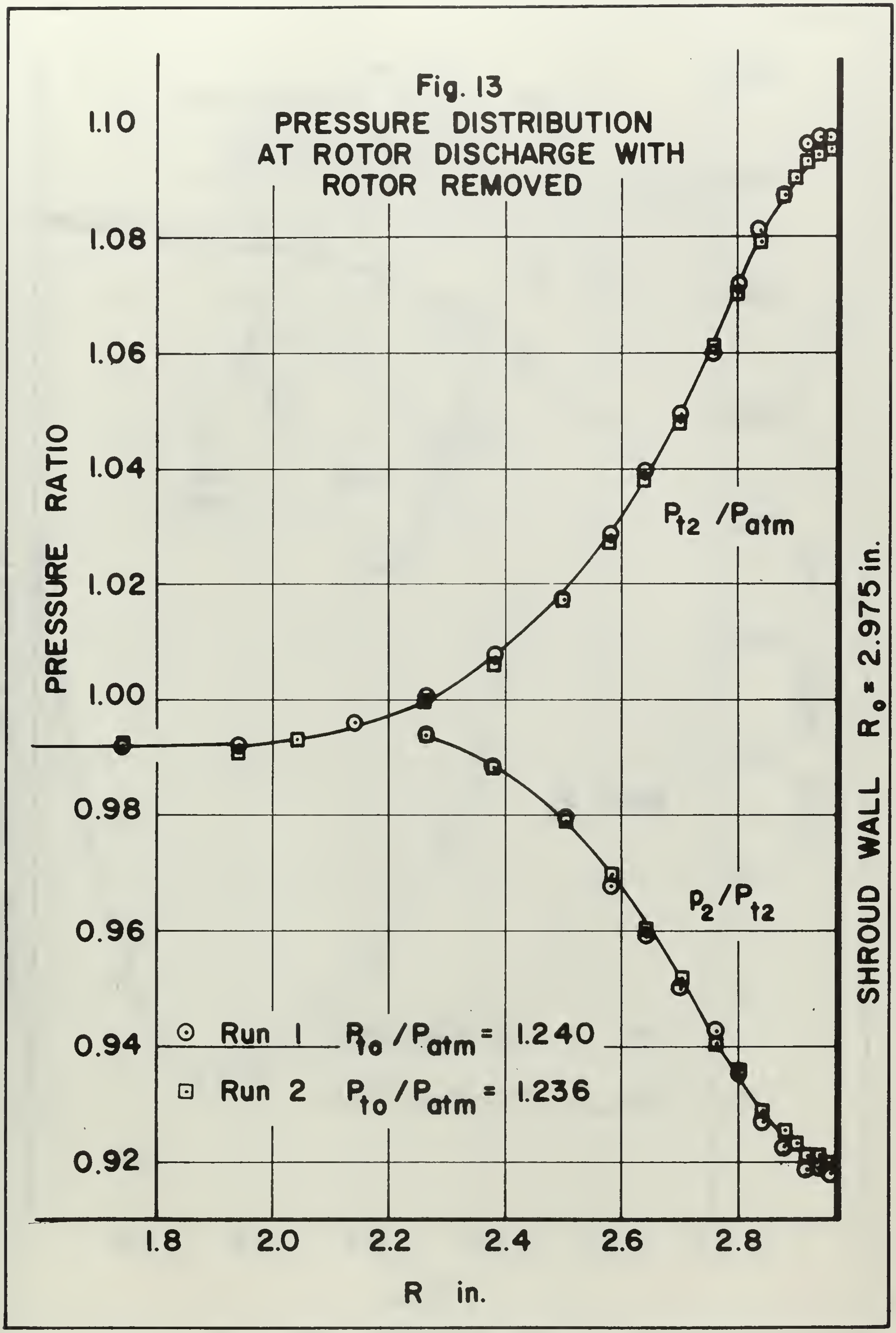
Fig. 13
PRESSURE DISTRIBUTION
AT ROTOR DISCHARGE WITH
ROTOR REMOVED
PRESSURE RATIO
1.10
1.08
1.06
1.04
1.02
1.00
0.98
0.96
0.94
0.92
P_{t2}/P_{atm}
p_2/P_{t2}
SHROUD WALL R_o = 2.975 in.
⊙ Run 1 P_{to}/P_{atm} = 1.240
⊡ Run 2 P_{to}/P_{atm} = 1.236
1.8
2.0
2.2
2.4
2.6
2.8
R in.

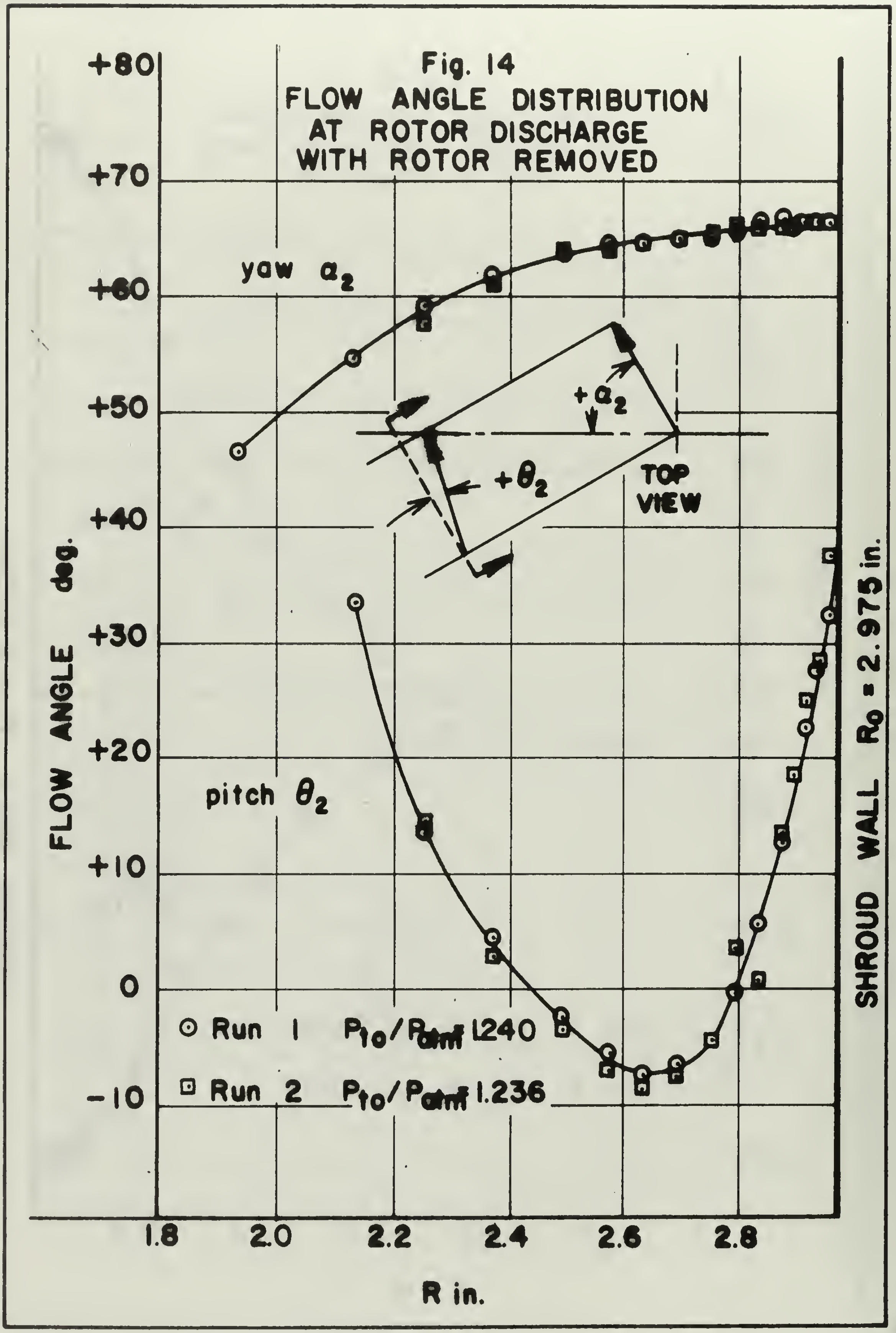

Fig. 14
FLOW ANGLE DISTRIBUTION
AT ROTOR DISCHARGE
WITH ROTOR REMOVED
yaw α_2
pitch θ_2
$+\alpha_2$
$+\theta_2$
TOP VIEW
FLOW ANGLE deg.
+80
+70
+60
+50
+40
+30
+20
+10
0
-10
1.8
2.0
2.2
2.4
2.6
2.8
R in.
SHROUD WALL $R_0 = 2.975$ in.
⊙ Run 1 $P_{to}/P_{atm} = 1.240$
⊡ Run 2 $P_{to}/P_{atm} = 1.236$

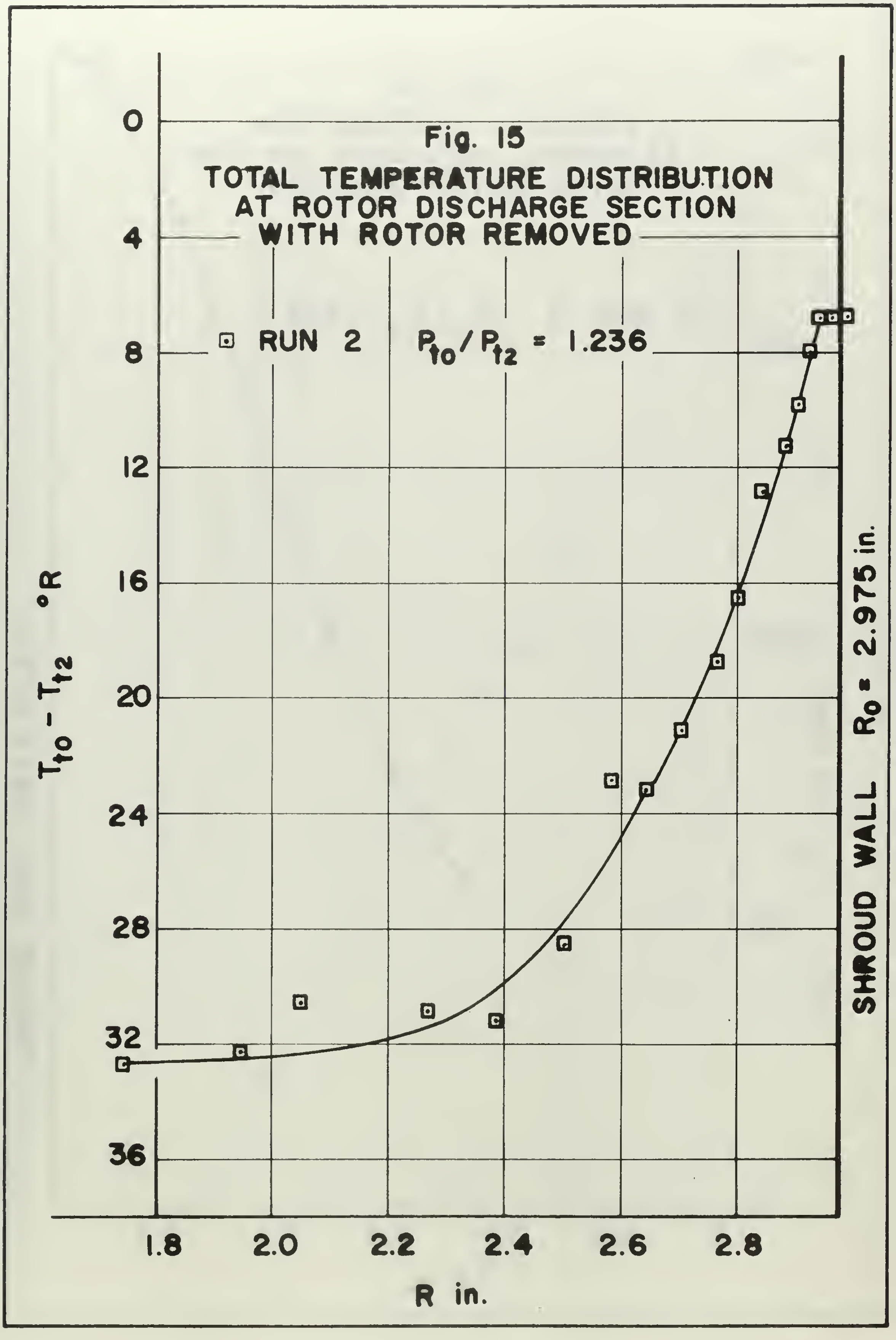
Fig. 15
TOTAL TEMPERATURE DISTRIBUTION
AT ROTOR DISCHARGE SECTION
WITH ROTOR REMOVED
RUN 2 P_{t0}/P_{t2} = 1.236
$T_{t0} - T_{t2}$ °R
0
4
8
12
16
20
24
28
32
36
1.8
2.0
2.2
2.4
2.6
2.8
R in.
SHROUD WALL R_0 = 2.975 in.

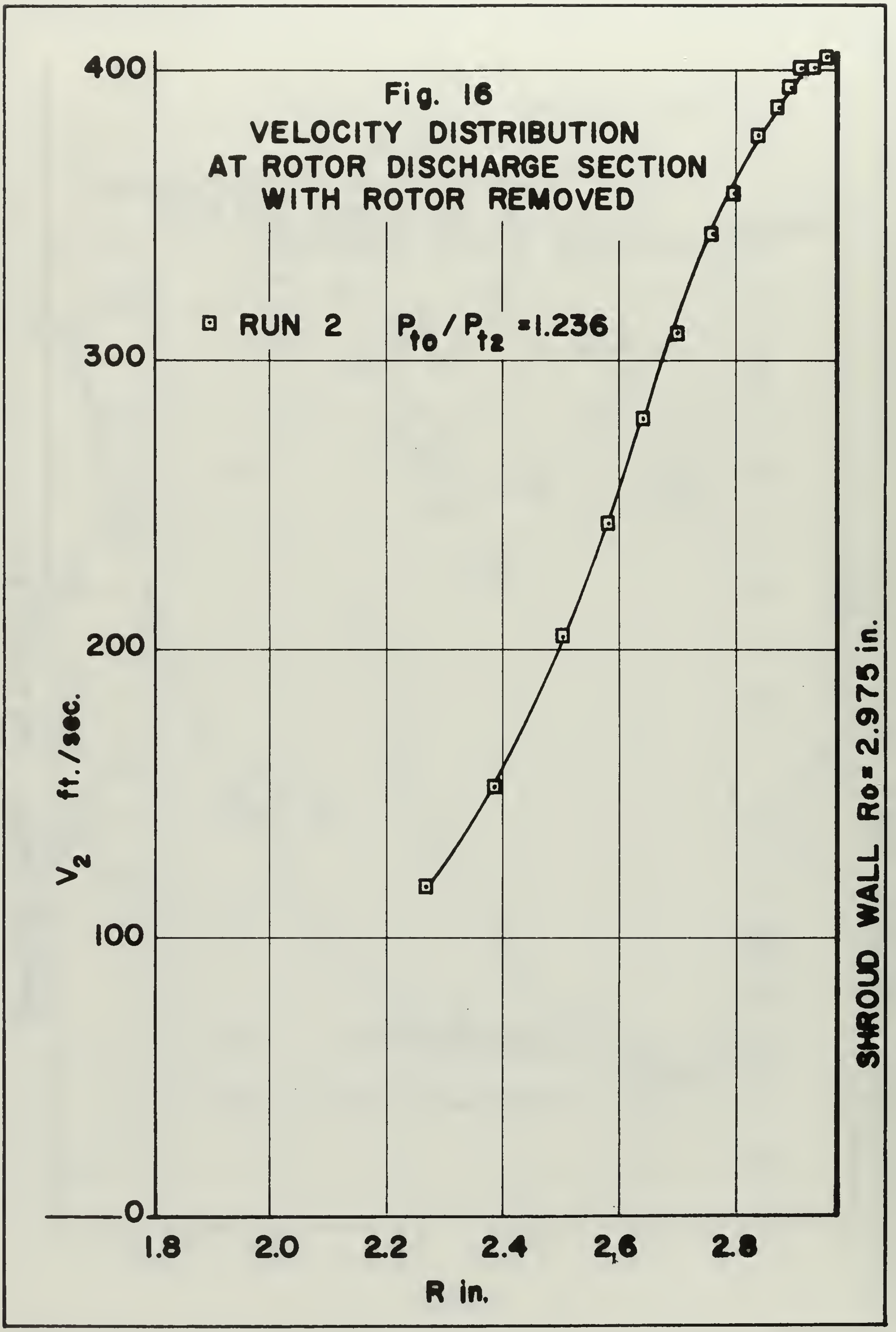

Fig. 16
VELOCITY DISTRIBUTION
AT ROTOR DISCHARGE SECTION
WITH ROTOR REMOVED
RUN 2 P_{to}/P_{t2} =1.236
400
300
200
100
0
V_2 ft./sec.
1.8
2.0
2.2
2.4
2.6
2.8
R in.
SHROUD WALL Ro= 2.975 in.

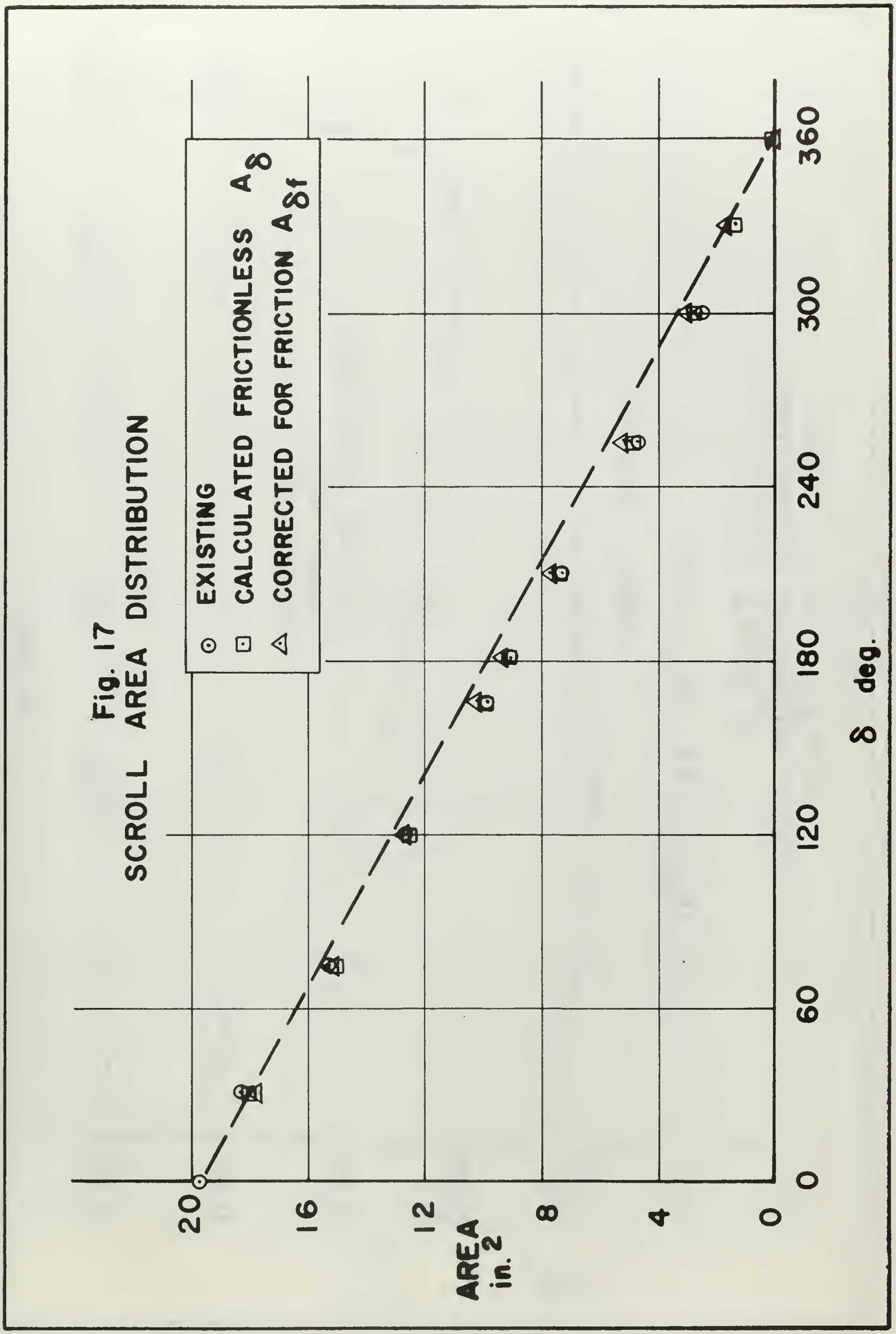

Fig. 17
SCROLL AREA DISTRIBUTION
EXISTING
CALCULATED FRICTIONLESS A_δ
CORRECTED FOR FRICTION $A_{\delta f}$
AREA in.^{2}
20
16
12
8
4
0
0
60
120
180
240
300
360
δ deg.

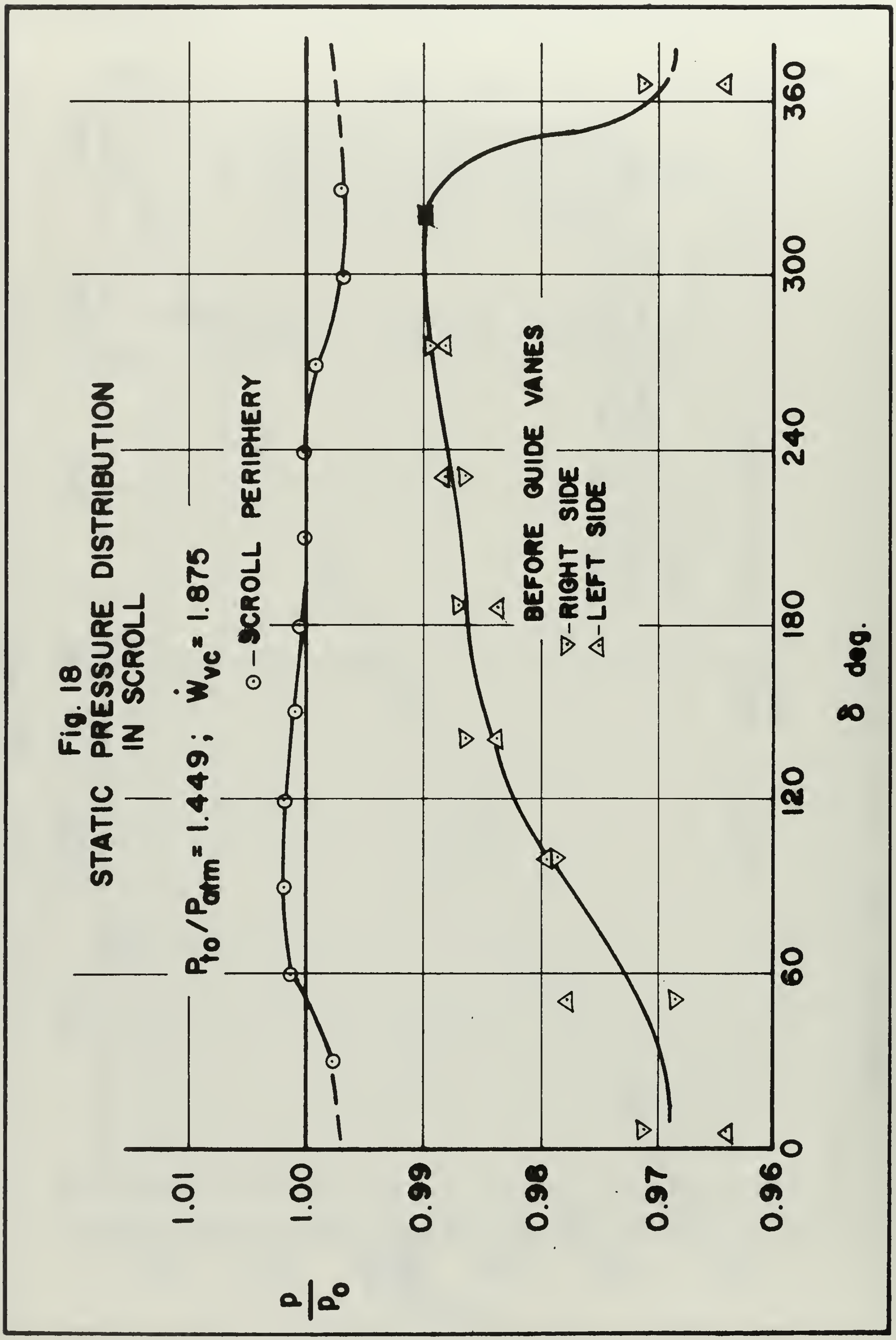

Fig. 18
STATIC PRESSURE DISTRIBUTION
IN SCROLL

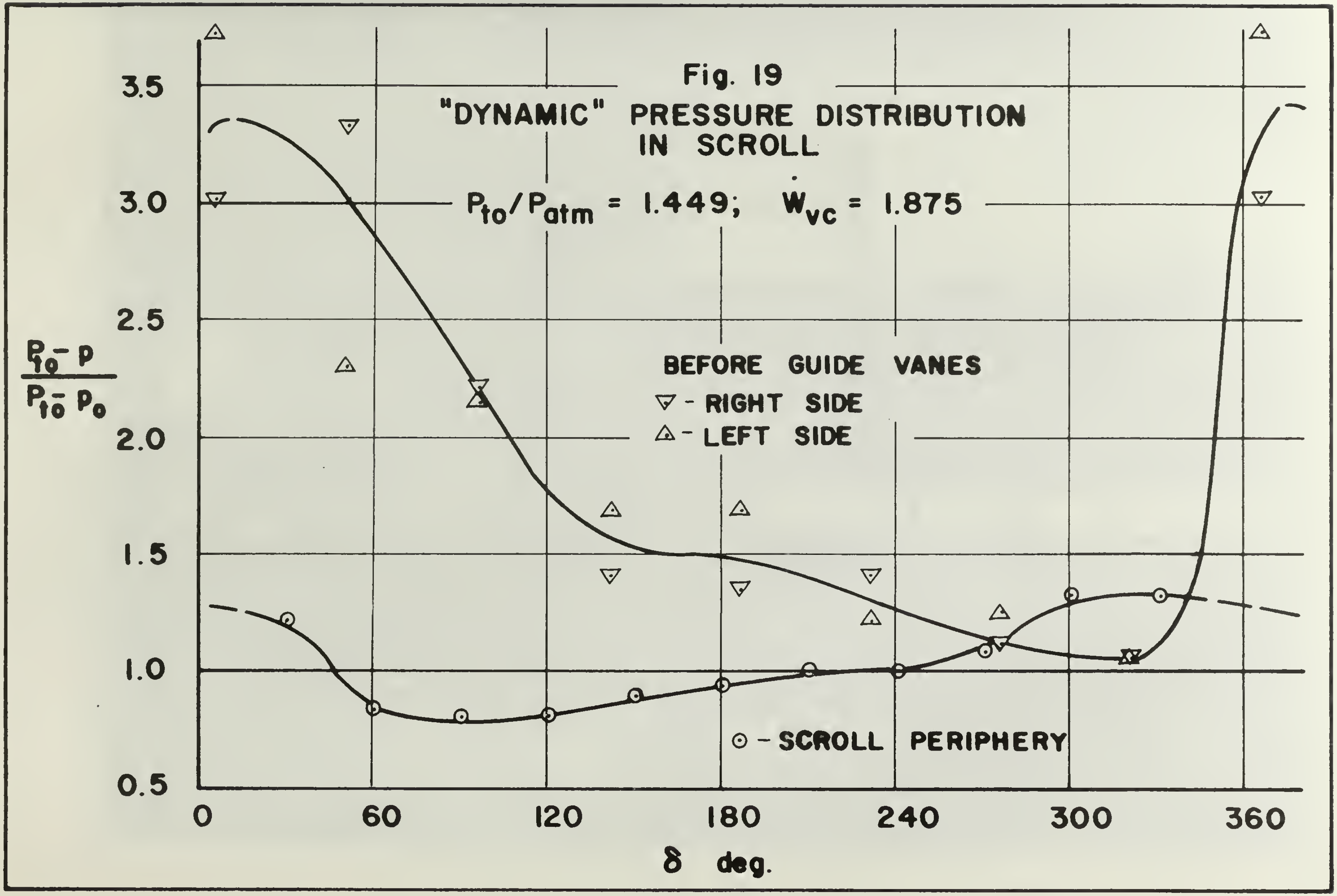

Fig. 19
"DYNAMIC" PRESSURE DISTRIBUTION IN SCROLL

$P_{to}/P_{atm} = 1.449; \quad \dot{W}_{vc} = 1.875$

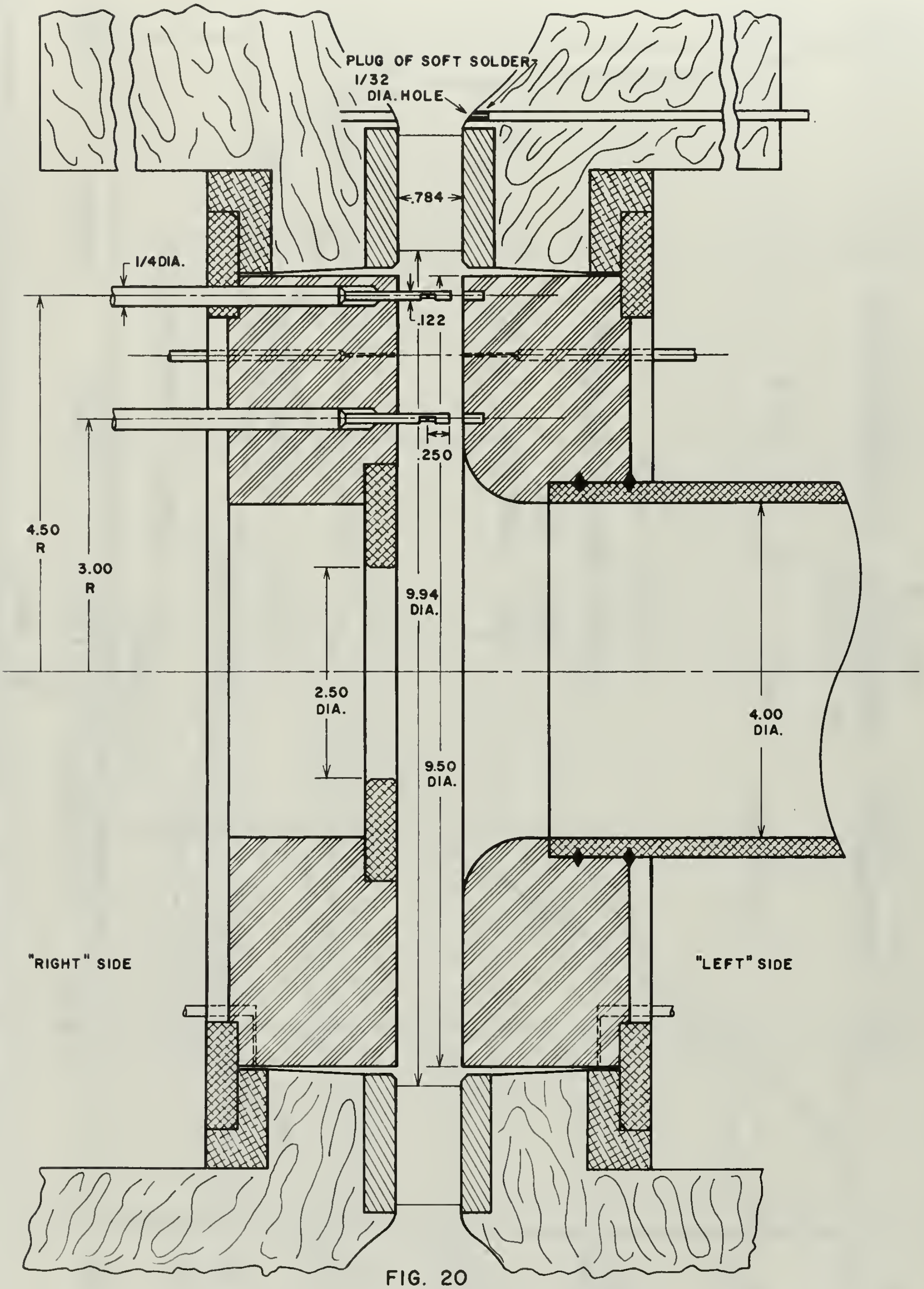

FIG. 20
CROSS SECTION OF VORTEX CHAMBER

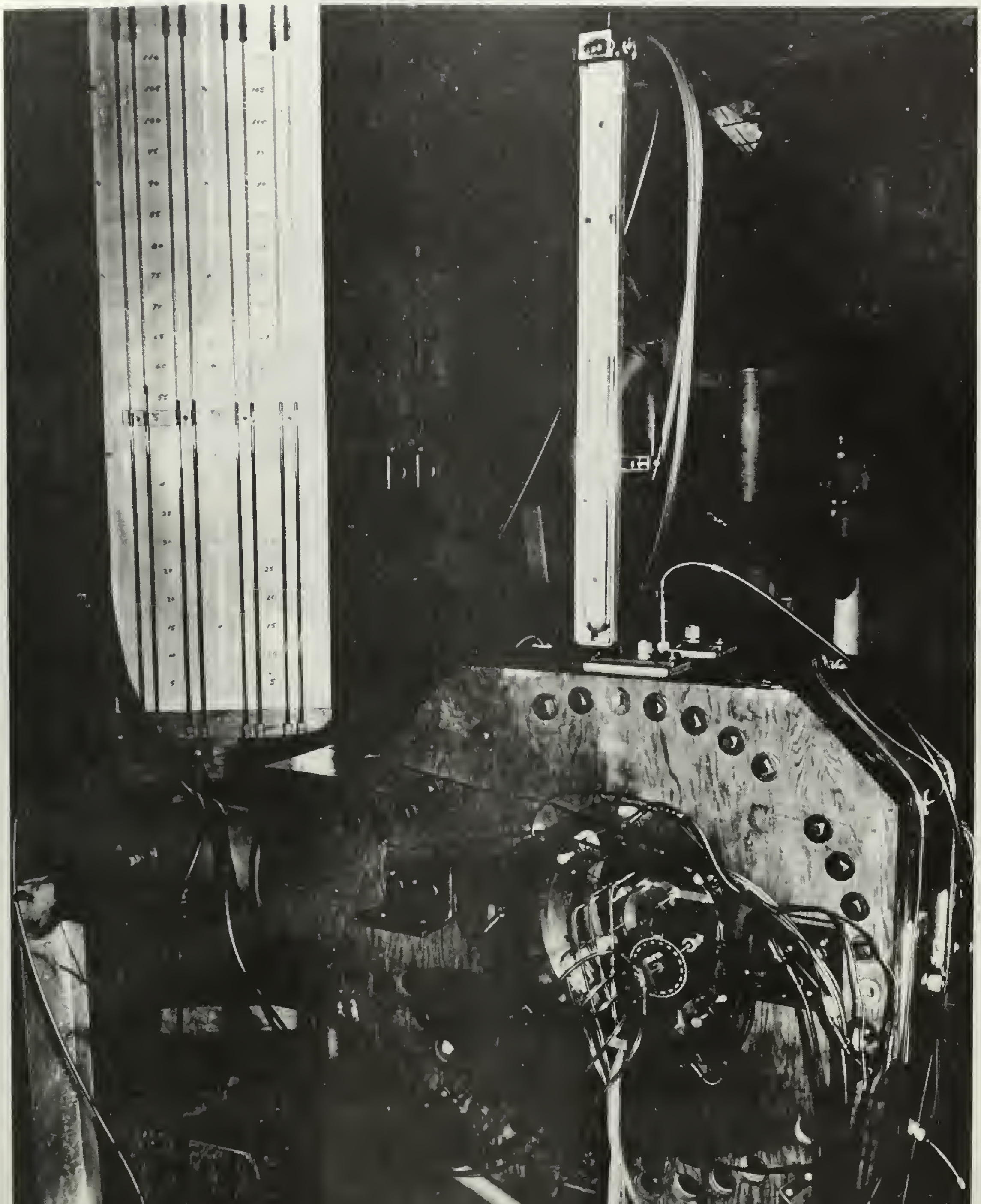

Fig. 21 Vortex Chamber Installation

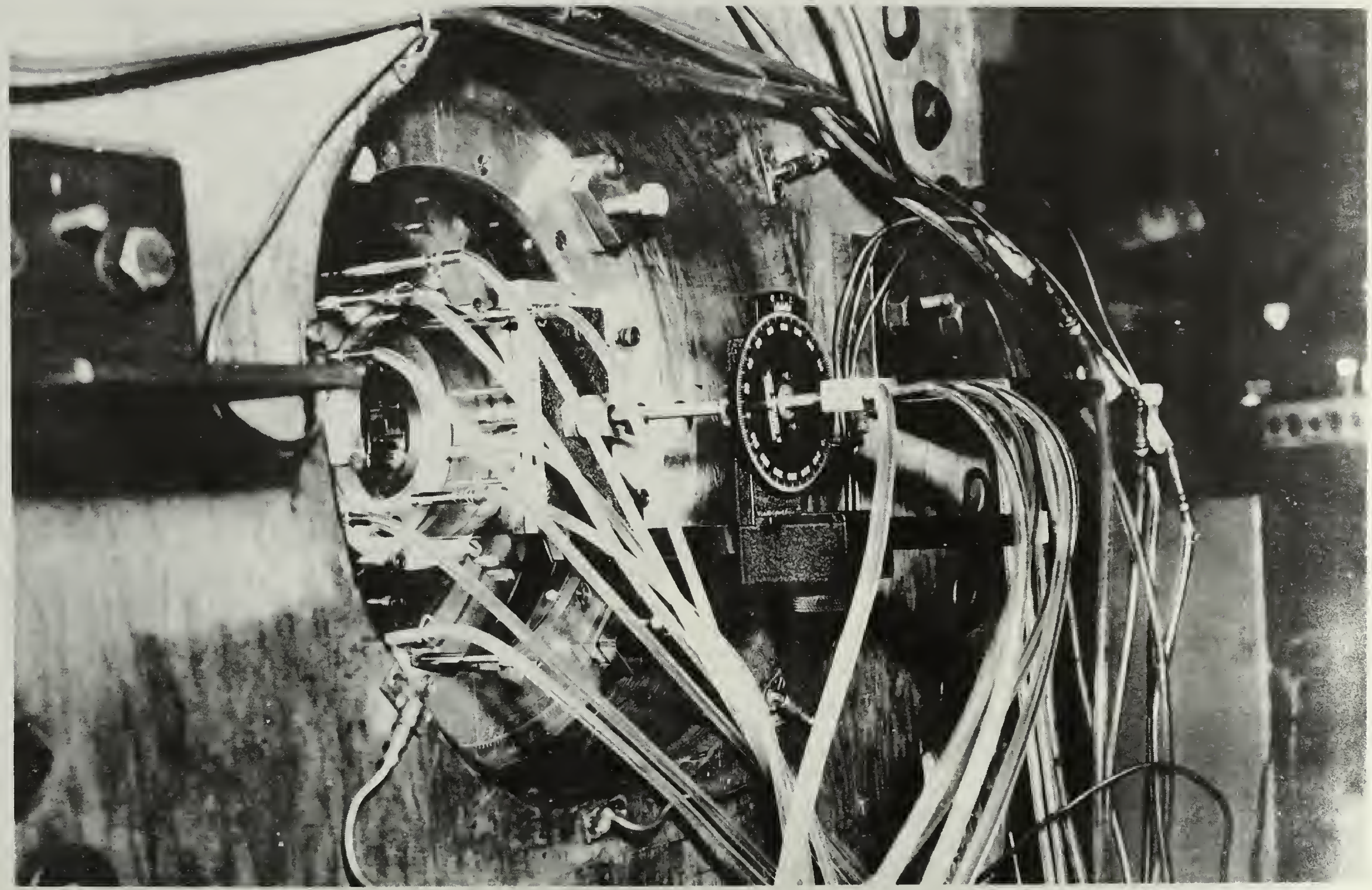

Fig. 22 Vortex Chamber Installation Close-up

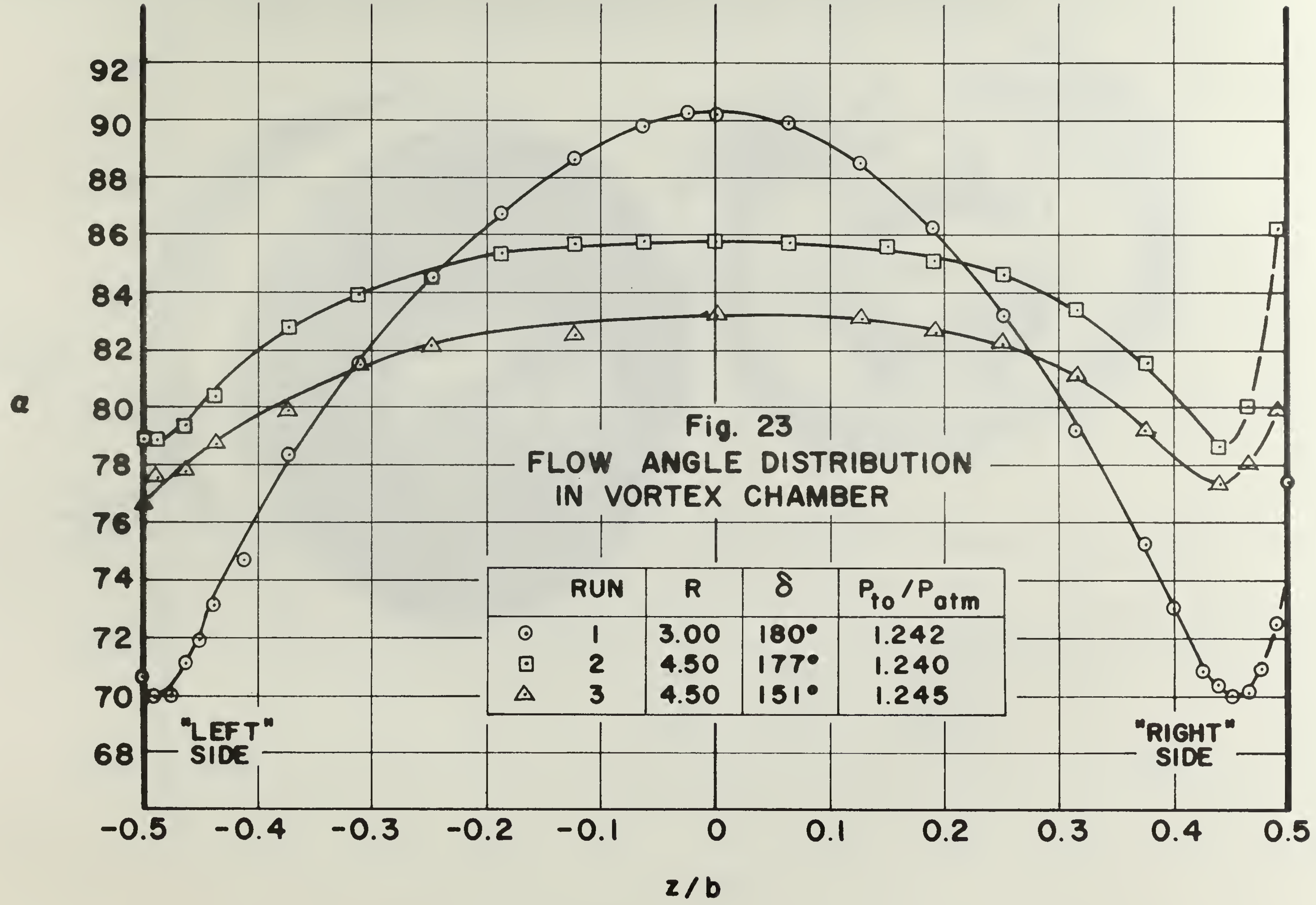

Fig. 23
FLOW ANGLE DISTRIBUTION
IN VORTEX CHAMBER

Fig. 24 Vortex Chamber Side Walls

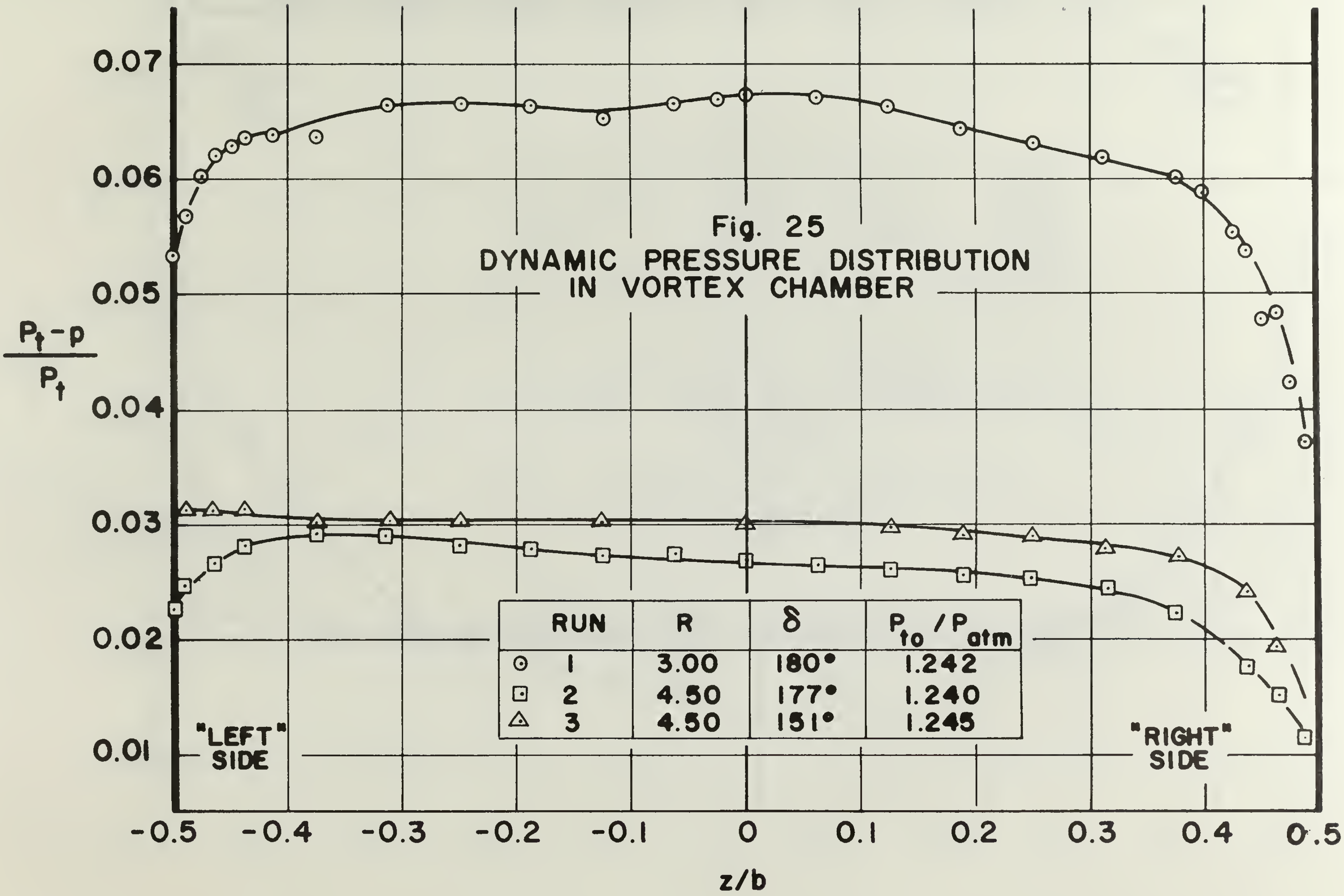

Fig. 25
DYNAMIC PRESSURE DISTRIBUTION IN VORTEX CHAMBER

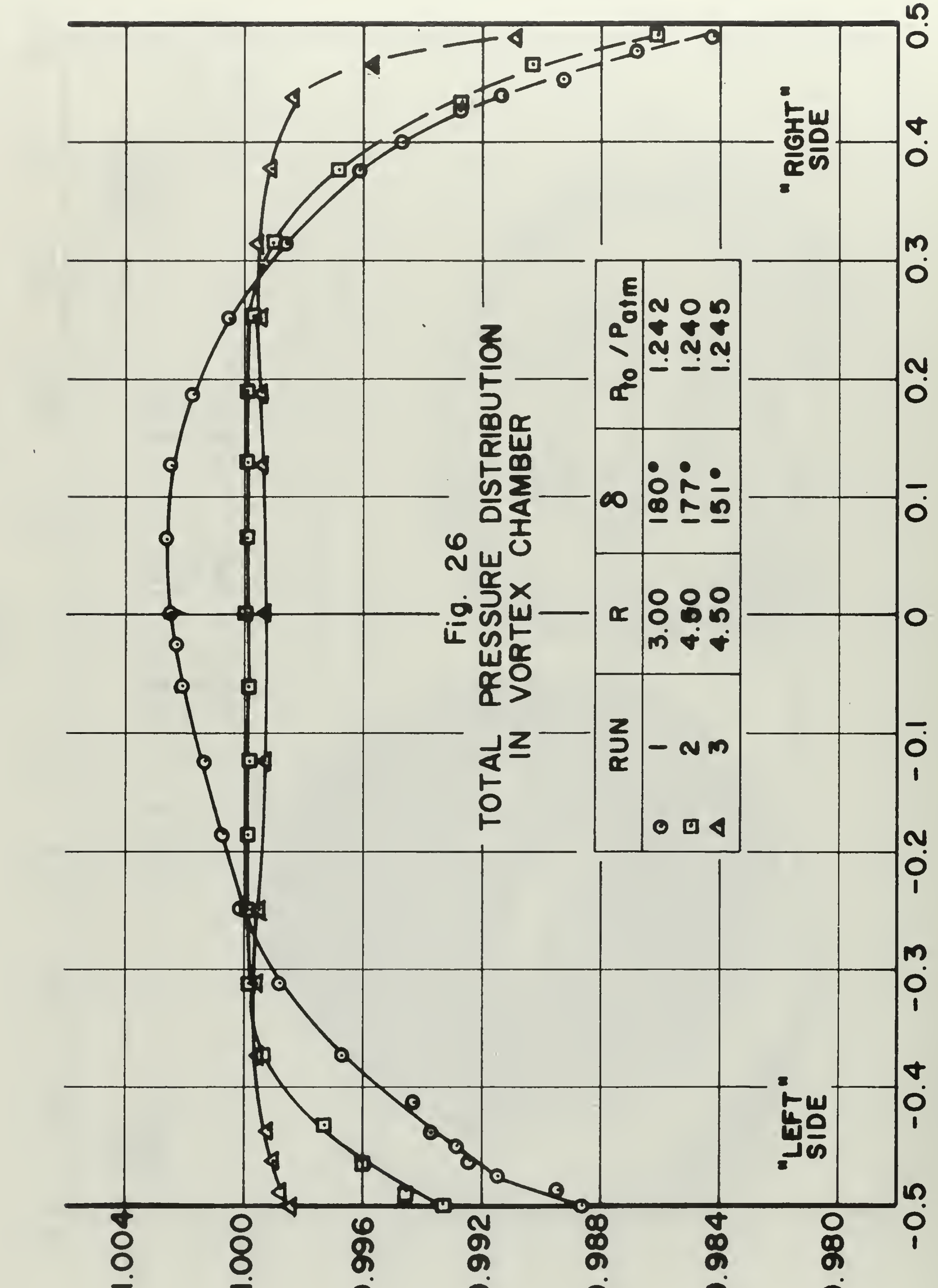

Fig. 26
TOTAL PRESSURE DISTRIBUTION IN VORTEX CHAMBER

	RUN	R	δ	P_{t0} / P_{atm}
⊙	1	3.00	180°	1.242
⊡	2	4.50	177°	1.240
△	3	4.50	151°	1.245

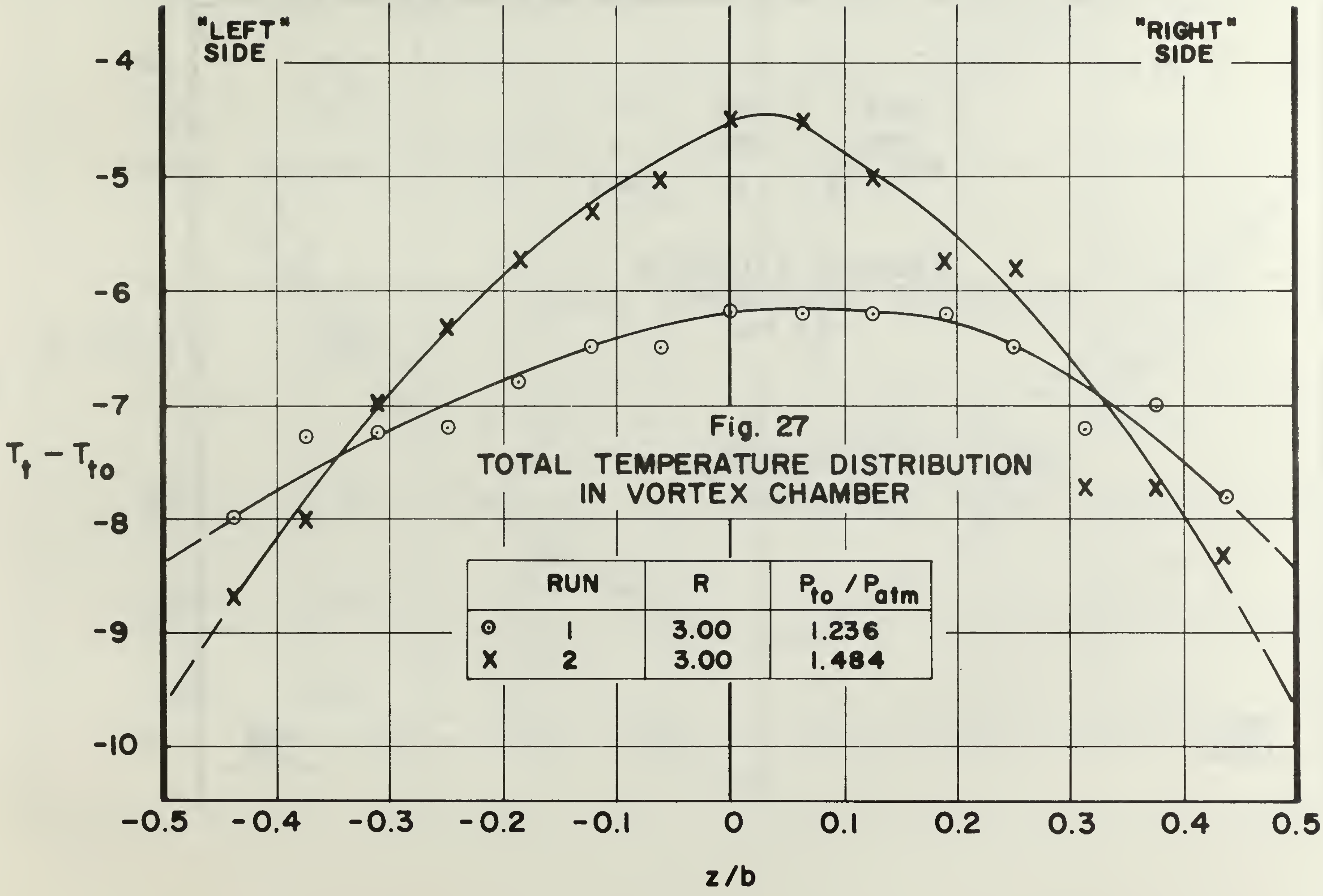

Fig. 27
TOTAL TEMPERATURE DISTRIBUTION IN VORTEX CHAMBER

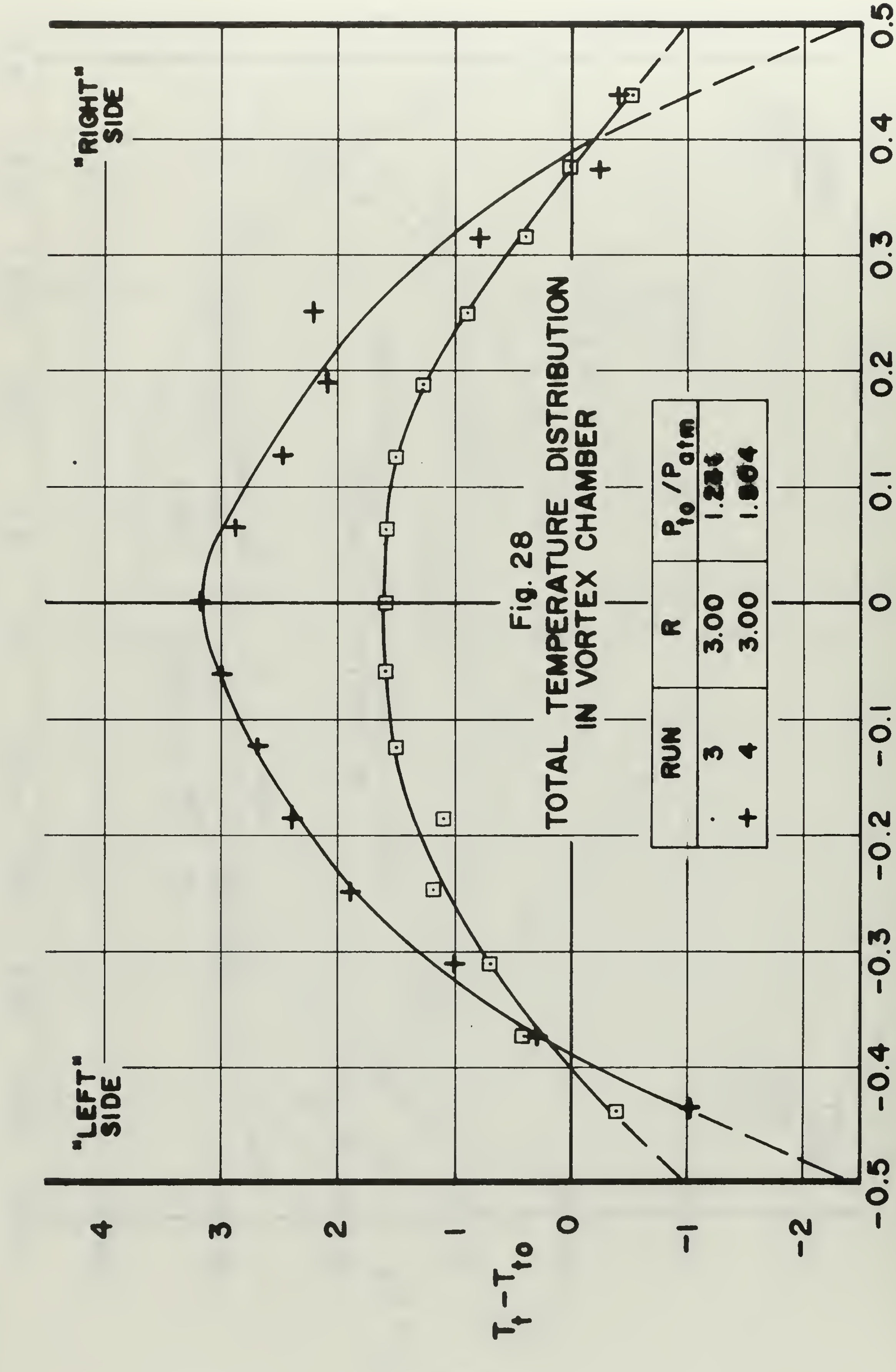

Fig. 28
TOTAL TEMPERATURE DISTRIBUTION IN VORTEX CHAMBER

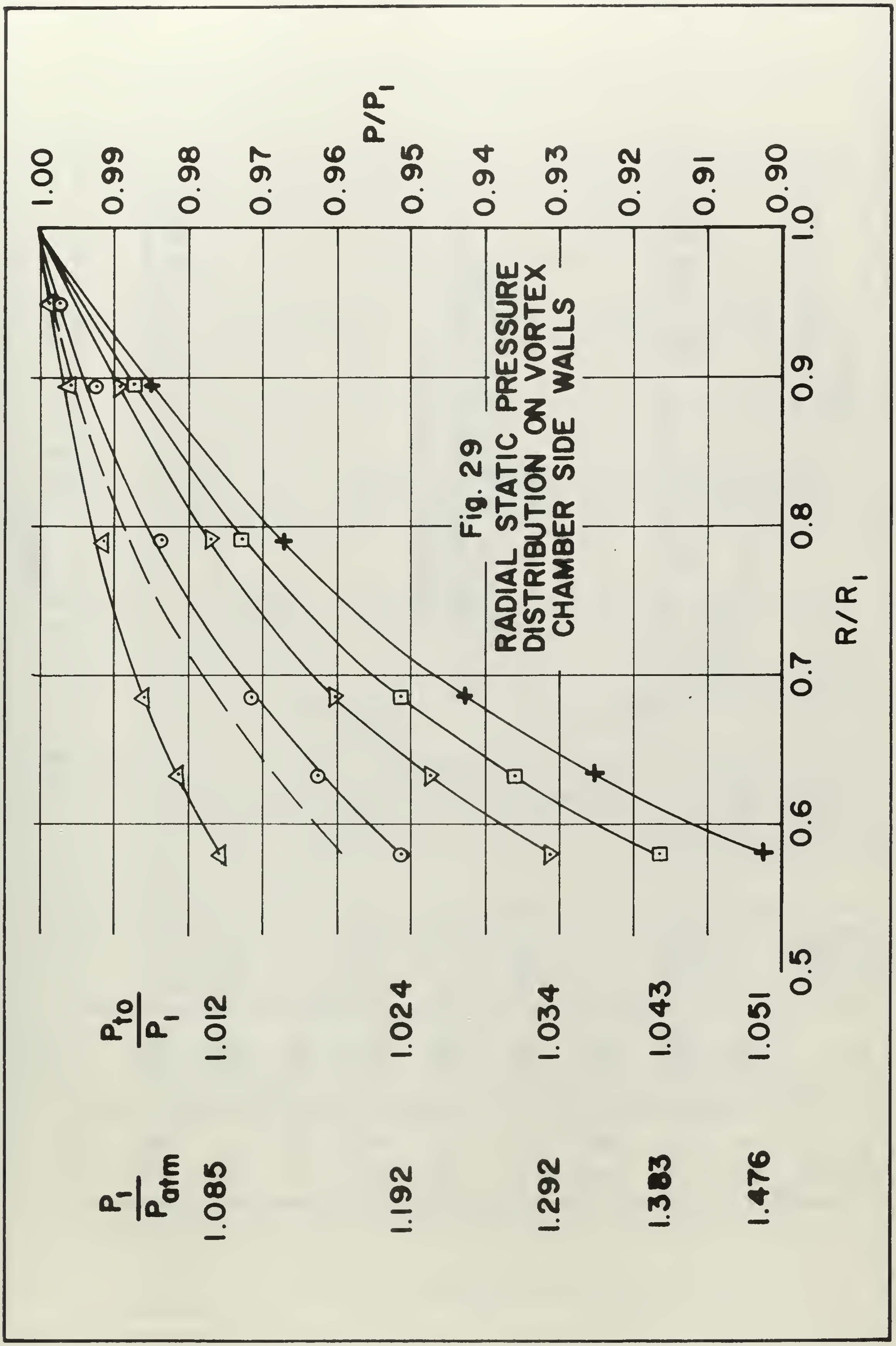

Fig. 29
RADIAL STATIC PRESSURE DISTRIBUTION ON VORTEX CHAMBER SIDE WALLS

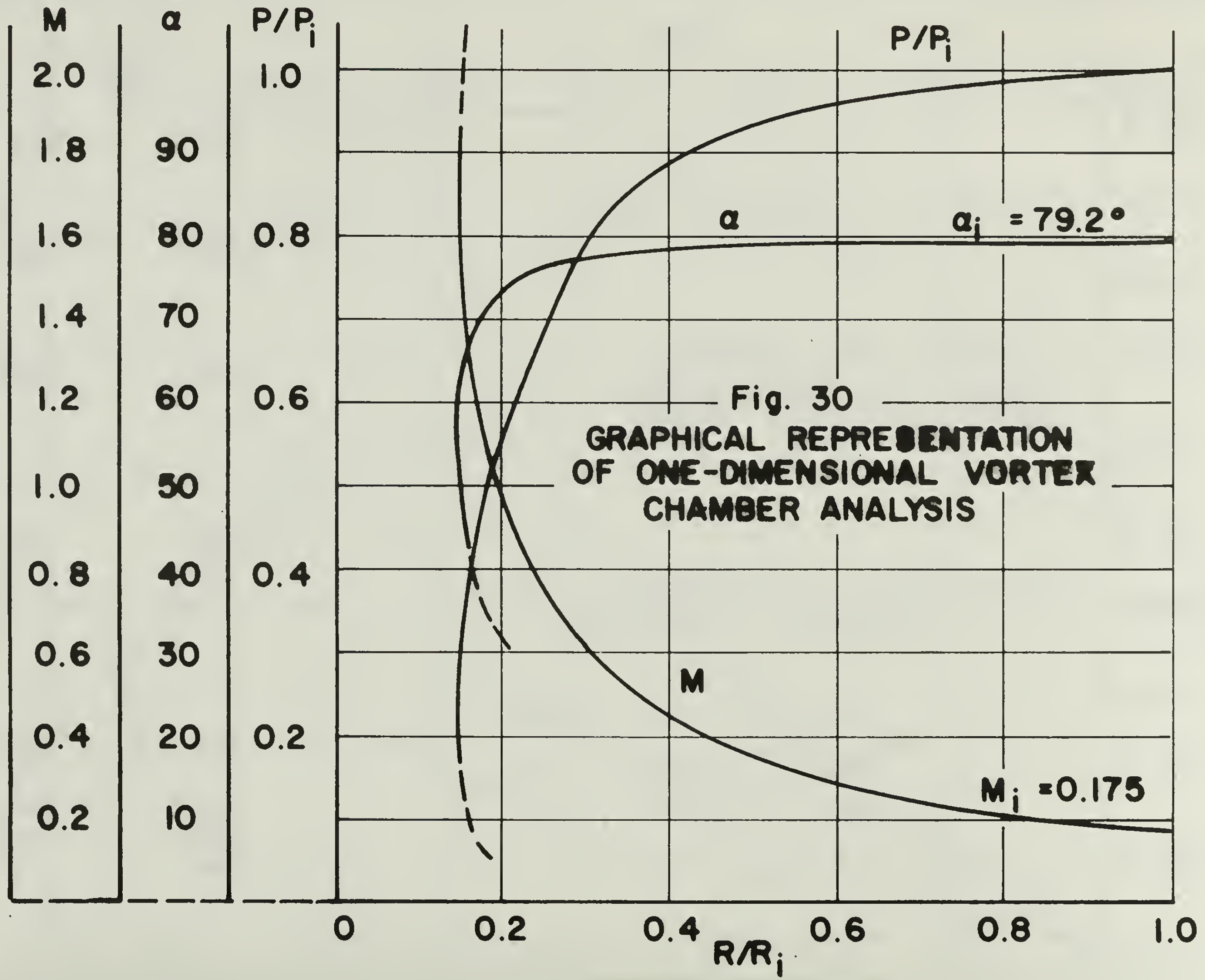

Fig. 30
GRAPHICAL REPRESENTATION OF ONE-DIMENSIONAL VORTEX CHAMBER ANALYSIS

8. References and Bibliography

1. Vavra, M. H. Private Communication of unpublished data, 1967

2. Riley, M. W. "The Effect of Axial Clearance on the Performance of a Dual Discharge Radial Turbine," Thesis, Naval Postgraduate School, 1966

3. Stearns, R. F. Flow Measurement with Orifice Meters. Van Nostrand, 1951

4. National Research Council International Critical Tables, Vol. III. McGraw-Hill, 1928

5. Keenan, J. M. and Kaye, J. Gas Tables. John Wiley and Sons, 1948

6. Shenker, H. Reference Tables for Thermocouples National Bureau of Standards, U.S. Department of Commerce, Circular 561, Government Printing Office, 1955

7. Vavra, M. H. Aero-Thermodynamics and Flow in Turbomachines. John Wiley and Sons, 1960

8. Vavra, M. H. Results of Turbine Air Testing Program, Phase II, Report ALGR-VA No. 29, for Aerojet General Corporation, 1965

9. Hartnett, J. P. and Eckert, E. R. G. "Experimental Study of the Velocity and Temperature Distribution in a High Velocity Vortex Type Flow," Heat Transfer and Fluid Mechanics Institute, Stanford University Press, 1956

10. Savino, J. M. and Ragsdale, R. G. "Some Temperature and Pressure Measurements in Confined Vortex Fields," Journal of Heat Transfer, February, 1961, Vol. 83, series C, no. 1, pp. 33-38

11. Deissler, R. G. and Perlmutter, M. "Flow and Energy Separation in a Turbulent Vortex," International Journal of Heat and Mass Transfer, August, 1960, Vol. 1, pp. 173-191

12. Vavra, M. H. von Karman Institute Lecture Series on Problems of Fluid Mechanics in Radial Turbomachines, Part I, March 1965

13. Eckert, B. Axial Kompressoren und Radial Kompressoren. Springer, Berlin, Germany, 1953

APPENDIX A

Program Scroll

Program SCROLL computes the losses in the scroll and guide vanes, and the absolute rotor inlet flow angle from torque, flow rate, and pressure data obtained in dummy rotor tests. The program is essentially that used by Riley [2] with several changes. The program can process any number of runs, with a maximum of ten sets of data per run. A block diagram of the program is shown in Fig. A1 and a program listing is given in Table A1.

A description of the main program and the subroutines is given below. The program initially reads the number of runs (NRUNS) which is used as an upper limit for the first DO loop. Within the DO loop, the number of sets of data (NSETS) and the input data for the run are read into the program. The input data is then printed out and the processing of each set of data is started using a DO loop with index K varying from 1 to NSET.

The value of the specific gravity of mercury G_{hg} at room temperature t_{rm} is determined by

$$G_{Hg} = 13.638 - 1.354(10^{-3})\,trm \qquad \text{(A-1)}$$

for temperatures between 0^{o}F and 150^{o}F. The factor for converting in. Hg to lb/ft^2 is

$$C_f = 69.892\,\frac{G_{Hg}}{13.59} \qquad \text{(A-2)}$$

The value of the specific gravity of water, G_{H2O}, at room temperature is

$$G_{H_2O} = 1.00013 + 7.8(10^{-5})t_{rm} - 1.4(10^{-6})t_{rm}^2 \quad \text{(A-3)}$$

The specific gravity relations were obtained from tabulated data of [4].

After the data for one run have been processed by the four subroutines, discussed in sections A1 through A4, the data are printed out and those for the next run are read into the program.

A1. Subroutine TEMP

Subroutine TEMP calculates the total temperature ahead of the flow measuring orifice, and at the manifold inlet, from chromel-alumel thermocouple readings. Using the measured voltage MV in milli-volts and the cold junction temperature t_{cj} the relations for the evaluation of the temperature in TEMP are

$$t = t_{cj} + 44.41MV + 0.2185MV^2 \quad \text{(A-4)}$$

for $t \leq 100^oF$

$$t = t_{cj} + 45.24MV - 0.3295MV^2 \quad \text{(A-5)}$$

for $100^oF < t \leq 200^oF$

Equations (A-4) and (A-5) were obtained from data tabulated in [6].

A2. Subroutine FLOW

Subroutine FLOW calculates the flow rate using only the pressures obtained with the vena-contracta taps of the orifice since this data gives a more accurate flow rate than flange tap data.[1] The flow rate is measured with a sharp edge orifice of 2.800 inch diameter which is installed in a pipe of 4.026 inch I.D.

The relation for the flow rate is[2]

$$\dot{W}_{VC} = C \, \alpha \, Y_1 \, F_r \sqrt{\frac{P_{1VC} \, \Delta h_{1VC}}{T_4}} \qquad \text{(A-6)}$$

where:

- C - factor dependent on orifice diameter, type of pressure taps, and dimensional units
- α - area multiplier to account for the thermal expansion of the orifice
- Y_1 - expansion factor to account for compressibility effects
- F_r - Reynolds number correction factor
- P_{1vc} - absolute pressure at upstream tap
- h_{1vc} - pressure differential across orifice
- T_4 - temperature ahead of the orifice

For vena-contracta taps[3] $C = 0.9057$

For a steel orifice[4]:

5

$$\alpha = 1 + (T_4 - 530)(10^{-3}) \qquad \text{(A-7)}$$

[1]Vavra, M. H., Results of Turbine Air Testing Program, Phase II, Report ALGER No. 29, for Aerojet General Corporation (1965), p. 219.

[2]Ibid., p. 220.

[3]Ibid., p. 221.

[4]Ibid., p. 220.

and

$$Y_1 = 1 - 0.351 \frac{\Delta h_{1vc}}{P_{1vc}} \tag{A-8}$$

$$F_r = 1 + \frac{0.00114}{X} \tag{A-9}$$

For an orifice diameter of 2.800 inches[5]

$$X = 0.812 \frac{\dot{W}_{vc}}{Z} \tag{A-10}$$

where for air between 50°F and 300°F

$$Z = 1.9 + 2.4(T_4 - 560)(10^{-3}) \tag{A-11}$$

Since F_r is nearly unity, the flow rate $\dot{W}_{vc}^*$ is determined first for $F_r = 1$. This flow rate is used to determine X by using Eq. (A-10), then the actual flow rate is taken as

$$\dot{W}_{vc} = F_r \dot{W}_{vc}^* \tag{A-12}$$

without further iteration.

P_{1vc} and Δh_{1vc} are converted to the proper units from their respective measured values by the relations

$$P_{1vc} = (P_{1vc}' - tare + 2.54 P_{atm}) \frac{G_{Hg}}{13.59} \tag{A-13}$$

and

$$\Delta h_{1vc} = (\Delta h_{1vc}' - tare) \frac{G_{Hg}}{13.59} \tag{A-14}$$

A3. Subroutine PRESS

Subroutine PRESS determines the static pressure ahead of the dummy rotor, and the ratio of the total pressure at

[5]Ibid., p. 220.

the manifold inlet and the static pressure ahead of the dummy rotor.

The static pressure at the rotor inlet p_1 is obtained from the average of the measured rotor inlet pressure $(h_{atm}-h_1)$, where h_1 is the average of the pressure readings, and h_{atm} is the reference pressure. Then

$$p_1 = \frac{(P_{atm})G_{Hg} + (h_{atm}-h_1)G_{H_2O}}{13.59} \qquad \text{(A-15)}$$

From the measured static pressure p_5' at the manifold inlet the absolute static pressure p_o at the inlet is

$$p_o = \left(\frac{p_5'-\text{tare}}{2.54} + P_{atm}\right)\frac{G_{Hg}}{13.59} \qquad \text{(A-16)}$$

An iteration process is used to determine an average value of the total pressure at the turbine inlet. Three relations are used in the iteration, namely, the gas law,

$$\rho_o = C_f \frac{p_o}{R_g T_o} \qquad \text{(A-17)}$$

the continuity equation,

$$V_o = \frac{\dot{W}_{vc}}{\rho_o A_5} \qquad \text{(A-18)}$$

and the energy equation,

$$T_o = T_{to} - \frac{V_o^2}{2gJc_p} \qquad \text{(A-19)}$$

where A_5 is the area of the five-inch pipe, and c_p is the specific heat of air at T_{to}. The variation of the specific heat at constant pressure c_p with temperature obtained from data tabulated in [5], is

$$c_p = 0.23943 + 3.4(10^{-6})t + 2(10^{-8})t^2 \qquad \text{(A-20)}$$

Using T_{to} for the first approximation of ρ_o, the iteration continues until a difference of 0.01°, or less, exists between any two successive values of T_o. Then the average total pressure P_{to} is

$$P_{to} = p_o + \frac{V_o^2}{2gC_f} \tag{A-21}$$

A4. Subroutine PSI

Subroutine PSI determines the inlet velocity coefficient ϕ and the absolute rotor inlet flow angle α_1.

From the theorem of angular momentum[1], for a steady flow that does not have a whirl component at the dummy rotor discharge ($V_{u2}=0$) the moment M exerted on the dummy rotor with radius 4.75 inches is

$$M = \dot{W}_{vc} \frac{4.75 V_{u1}}{g} \tag{A-22}$$

The moment M equals the product of the scale reading F and the length of the moment (12 inches). Thus the peripheral component of the absolute rotor inlet velocity V_1 is from Eq. (A-22)

$$V_{u1} = \frac{12 Fg}{4.75 \dot{W}_{vc}} \tag{A-23}$$

The velocity coefficient ϕ is determined by an iteration using the rotor inlet velocity V_1. The first approximation to V_1 is obtained by assuming an isentropic expansion from the manifold inlet total pressure P_{to} to the rotor inlet pressure p_1; that is, the velocity coefficient ϕ is

[1]Vavra, M. H. Aero-Thermodynamics and Flow in Turbomachines (John Wiley and Sons, 1960), p. 98.

set equal to unity, and

$$V_1 = \sqrt{2gJc_pT_{to}\left[1-\left(\frac{p_1}{P_{to}}\right)^{\frac{\gamma-1}{\gamma}}\right]} \qquad \text{(A-24)}$$

The variation with temperature of the ratio of specific heats γ obtained from data tabulated in [5] is

$$\gamma = 1.4018 - 2(10^{-5})t \qquad \text{(A-25)}$$

The meridional component of V_1 is

$$V_{m1} = \sqrt{V_1^2 - V_{u1}^2} \qquad \text{(A-26)}$$

Using the continuity equation, the density ρ_1 is

$$\rho_1 = \frac{\dot{W}_{vc}}{A_1 V_{m1}} \qquad \text{(A-27)}$$

where the meridional cross-sectional area A_1 is

$$A_1 = \frac{\pi(9.5)B_1}{144} \qquad \text{(A-28)}$$

B_1 is the distance between the shrouds at the dummy rotor tip radius of 4.75 inches and depends on the axial clearance used for the test. Using the gas law, the static inlet temperature T_1 is

$$T_1 = C_f \frac{p_1}{\rho_1 R_g} \qquad \text{(A-29)}$$

The second approximation of V_1 is

$$V_1 = \sqrt{2gJc_p(T_{to}-T_1)} \qquad \text{(A-30)}$$

By reducing ϕ in increments of 0.0001 until the two approximations for V_1 agree within 1.0 ft/sec. the actual value of 0.5 ϕ is obtained.

The absolute rotor inlet flow angle α_1 is then

$$\alpha_1 = \tan^{-1} \frac{V_{u1}}{V_{m1}} \qquad \text{(A-31)}$$

From the velocity V_1 and the static temperature T_1, the Mach number M_1 at the rotor inlet is

$$M_1 = \frac{V_1}{\sqrt{\gamma R_g g T_1}} \qquad \text{(A-32)}$$

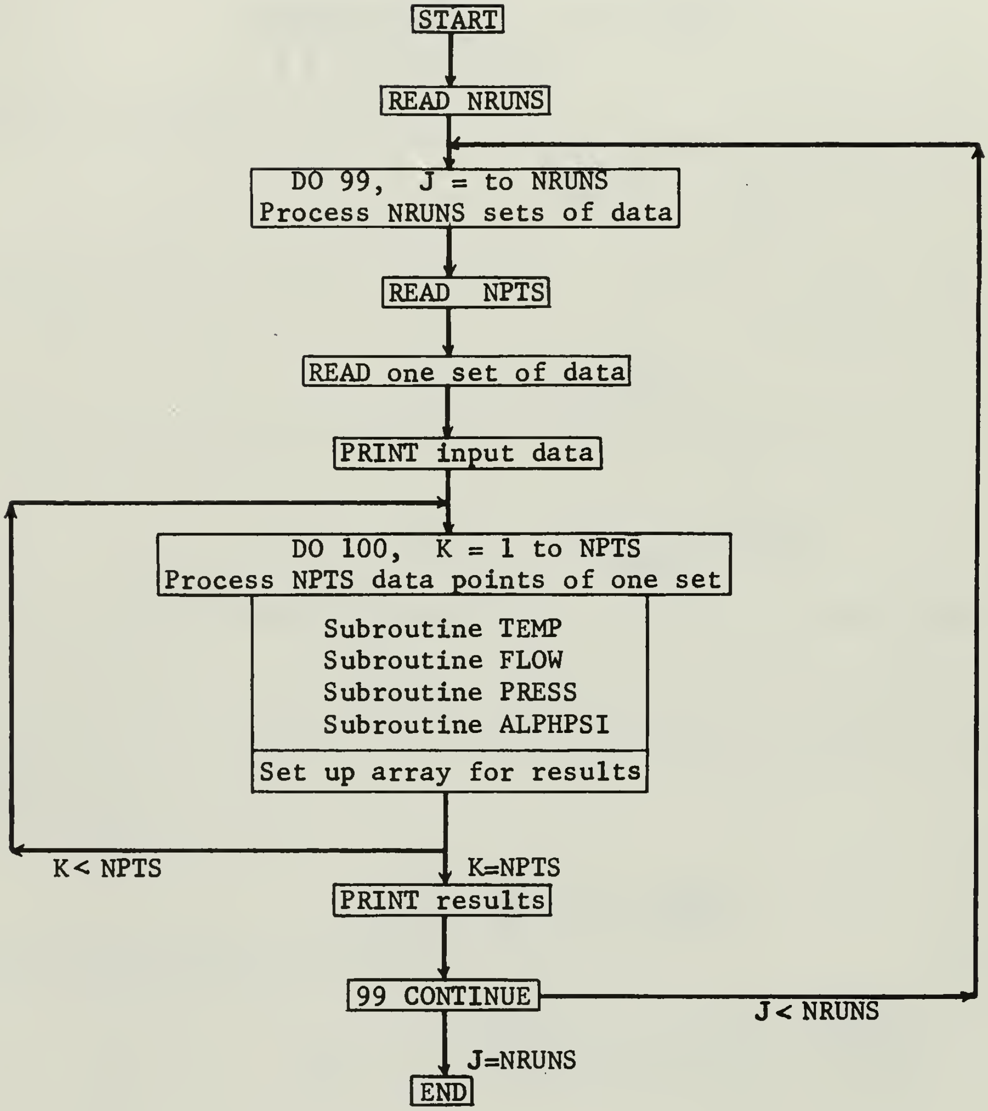

Fig. A1

Block Diagram of Program SCROLL

Table A1 Program SCROLL Listing

```
-COOP,,BOSHOVEN,S/1S/2S,5,1000.
-FTN,L,E.
C     PROGRAM SCROLL
      DIMENSION DPVC(10),PUVC(10),P5P(10),PATM(10),HATM(10),H1(10),
     1SR(10),TRM(10),V4(10),V5(10),WVCP(10),PRP(10),PHIP(10),ALPH(10),
     2VEL(10),TS(10),ACH(10),PS(10)
      COMMON GHG,GWR,CF1,TCJ,TARE,STARE,T4,T5,WVC,PR,P1,PHI,ALP1,PAT,
     1V1,T1,ACH1,B1
      READ 10,NRUNS
      DO 99 J=1,NRUNS
      READ 10,NPTS
      READ 11,(DPVC(K),PUVC(K),P5P(K),PATM(K),HATM(K),H1(K),SR(K),TRM(K)
     1,V4(K),V5(K),K=1,NPTS)
      READ 12,TCJ,TARE,STARE,B1
      PRINT 20
      PRINT 21,(K,DPVC(K),PUVC(K),P5P(K),PATM(K),HATM(K),H1(K),SR(K),TRM
     1(K),V4(K),V5(K),K=1,NPTS)
      PRINT 24,TCJ,TARE,STARE,B1
      DO 100 K=1,NPTS
      GHG=13.638-1.354E-3*TRM(K)
      GWR=1.00013+7.8E-5*TRM(K)-1.4E-6*TRM(K)**2
      CF1=69.892*GHG/13.59
      DPV=DPVC(K)
      PUV=PUVC(K)
      P5=P5P(K)
      PAT=PATM(K)
      HAT=HATM(K)
      P1P=H1(K)
      S=SR(K)
      V4T=V4(K)
      V5T=V5(K)
      CALL TEMP (V4T,V5T)
      CALL FLOW (DPV,PUV)
      CALL PRESS (P5,HAT,P1P)
      CALL ALPHPSI (S)
      WVCP(K)=WVC
```

Table A1 (Cont.)

```
      PRP(K)=PR
      PHIP(K)=PHI
      ALPH(K)=ALP1
      VEL(K)=V1
      TS(K)=T1
      ACH(K)=ACH1
      PS(K)=P1
  100 CONTINUE
      PRINT 22
      PRINT 23,(K,PRP(K),WVCP(K),PHIP(K),ALPH(K),
     1VEL(K),TS(K),ACH(K),PS(K),K=1,NPTS)
   99 CONTINUE
      PRINT 25
   10 FORMAT(I4)
   11 FORMAT(10F7.2)
   12 FORMAT(3F7.2,F6.3)
   20 FORMAT(1H1//2X14HPROGRAM SCROLL50X13HR.L. BOSHOVEN//15X49HSCROLL A
     1ND GUIDE VANE TESTS OF ICP RADIAL TURBINE//27X23HTABLE        INPU
     2T DATA /// 2X 73H  PT   DPVC   PUVC   P5P   PATM   HATM   H1
     3 SR    TRM     V4      V5/)
   21 FORMAT(I6,10F7.2)
   22 FORMAT(1H1//2X14HPROGRAM SCROLL50X13HR.L. BOSHOVEN//15X49HSCROLL A
     1ND GUIDE VANE TESTS OF ICP RADIAL TURBINE//27X24HTABLE        OUTP
     2UT DATA/// 2X71H  PT   PTO/P1   WVC      PHI    ALPH(1)   V1
     3 T1      MACH1     P1/)
   23 FORMAT(I6,2F8.3,F8.4,3F9.2,2F9.3)
   24 FORMAT(/9X5HTCJ -F6.2,6X6HTARE -F4.2,6X7HSTARE -F5.2,6X4HB1 -F6.3)
   25 FORMAT(1H1)
      END
C
      SUBROUTINE TEMP (V4,V5)
      COMMON GHG,GWR,CF1,TCJ,TARE,STARE,T4,T5,WVC,PR,P1,PHI,ALP1,PAT,
     1V1,T1,ACH1,B1
      V=V4
      J=1
  100 T = TCJ + 44.41 * V + .2185 * V ** 2
```

Table A1 (Cont.)

```
      IF( T - 100.) 102,102,101
  101 T = TCJ + 45.24 * V - .3295 * V ** 2
  102 T=T+459.7
      IF(J-1)103,103,104
  103 J=2
      T4=T
      V=V5
      GO TO 100
  104 T5=T
      RETURN
      END
C
      SUBROUTINE FLOW (DPVC,PUVC)
      COMMON GHG,GWR,CF1,TCJ,TARE,STARE,T4,T5,WVC,PR,P1,PHI,ALP1,PAT,
     1V1,T1,ACH1,B1
      DVC=(DPVC-TARE)*GHG/13.59
      PVC=(PUVC-TARE+PAT *2.54)*GHG/13.59
      A=1.+1.E-5*(T4-530.)
      Z=1.9+2.4E-3*(T4-560.)
      Y=1.-.351*DVC/PVC
      WVC=.9057*A*Y*SQRTF(PVC*DVC/T4)
      X=WVC*.812/Z
      WVC=(1.+.00114/X)*WVC
      RETURN
      END
C
      SUBROUTINE PRESS(P5P,HAT,H1)
      COMMON GHG,GWR,CF1,TCJ,TARE,STARE,T4,T5,WVC,PR,P1,PHI,ALP1,PAT,
     1V1,T1,ACH1,B1
      A=T5-459.7
      CP=.23943+3.4E-6*A+2.E-8*A**2
      P1=(PAT*GHG+(HAT-H1)*GWR)/13.59
      PS5=(PAT +(P5P-TARE)/2.54)*GHG/13.59
      TT=T5
  100 RHO=PS5*CF1/(TT*53.35)
      V0=WVC/(RHO*3.14159*6.25/144.)
```

Table A1 (Cont.)

```
      T0=T5-(V0**2)/(2.*32.174*778.16*CP)
      DTT=TT-T0
      TT=T0
      IF(ABSF(DTT)-.01)101,101,100
  101 PT0=PS5+RHO*(V0**2)/(2.*32.174*CF1)
      PR=PT0/P1
      RETURN
      END
C
      SUBROUTINE ALPHPSI (SR)
      COMMON GHG,GWR,CF1,TCJ,TARE,STARE,T4,T5,WVC,PR,P1,PHI,ALP1,PAT,
     1V1,T1,ACH1,B1
      T=T5-459.7
      GAM=1.4018-2.E-5*T
      EXP=(GAM-1.)/GAM
      CP=.23943+3.4E-6*T+2.E-8*T**2
      G=2.*32.174*778.16*CP
      RM=(SR-STARE)*12.0
      VU1=RM*32.174/(WVC*4.75)
      B=T5*(1.-1./PR**EXP)
      A1=2.*3.14159*4.75*B1/144.
      PHI=1.
  100 V1=PHI*SQRTF(G*B)
      T1=T5-(V1**2)/G
      RHO=P1*CF1/(T1*53.35)
      VM1=WVC/(A1*RHO)
      V1A=SQRTF(VM1**2+VU1**2)
      IF(ABSF(V1-V1A)-.5)102,102,101
  101 PHI=PHI-.0001
      GO TO 100
  102 ALP1=57.29578*ATANF(VU1/VM1)
      ACH1=V1/SQRTF(32.174*GAM*53.35*T1)
      RETURN
      END
      END
         FINIS
```

PROGRAM SCROLL R.L. BOSHOVEN

SCROLL AND GUIDE VANE TESTS OF ICP RADIAL TURBINE

TABLE A2 INPUT DATA RILEY (2)

PT	DPVC	PUVC	P5P	PATM	HATM	H1	SR	TRM	V4	V5
1	10.56	25.56	14.83	30.02	56.50	49.11	8.68	72.00	1.99	1.92
2	11.55	28.15	16.47	30.02	56.50	48.31	9.46	73.00	1.86	1.83
3	12.77	31.54	18.51	30.02	56.50	47.26	10.39	73.00	1.82	1.78
4	13.72	34.01	20.05	30.02	56.50	46.42	11.17	73.00	1.82	1.78
5	15.03	37.41	22.12	30.02	66.00	54.21	12.14	74.50	1.90	1.87
6	17.21	43.35	25.93	30.02	60.20	47.26	13.95	74.00	1.87	1.83
7	19.15	48.99	29.40	30.02	66.10	50.39	15.50	74.00	1.90	1.86
8	23.16	60.57	36.89	30.02	66.10	47.25	19.03	74.00	1.95	1.91

TCJ - 32.00 TARE - 0 STARE - 1.45 B1 - .943

SCROLL AND GUIDE VANE TESTS OF ICP RADIAL TURBINE

TABLE A2 OUTPUT DATA RILEY (2)

PT	PTO/P1	WVC	PHI	ALPH(1)	V1	T1	MACH1	P1
1	1.180	1.187	.8884	80.26	502.86	556.31	.435	30.454
2	1.200	1.260	.8889	80.22	525.03	550.45	.457	30.509
3	1.223	1.344	.8863	80.13	549.38	546.07	.480	30.586
4	1.241	1.405	.8907	80.13	571.03	544.06	.499	30.648
5	1.264	1.484	.8900	80.00	594.83	545.72	.520	30.769
6	1.310	1.624	.8893	79.91	635.95	539.74	.558	30.855
7	1.347	1.745	.8873	79.74	665.55	537.86	.586	31.059
8	1.433	1.990	.8881	79.53	730.83	532.48	.646	31.289

SCROLL AND GUIDE VANE TESTS OF ICP RADIAL TURBINE

TABLE A3 INPUT DATA Run 1

PT	DPVC	PUVC	P5P	PATM	HATM	H1	SR	TRM	V4	V5
1	5.23	12.48	7.23	30.22	50.10	45.81	4.99	75.00	2.18	2.07
2	5.54	13.32	7.62	30.22	50.10	45.55	5.23	75.00	2.21	2.12
3	7.84	19.31	11.20	30.22	50.10	43.38	6.95	75.00	2.25	2.17
4	12.77	32.71	19.70	30.22	50.15	38.67	10.94	74.00	2.27	2.21
5	15.53	40.45	24.66	30.22	50.25	36.17	13.26	74.00	2.34	2.30
6	17.74	47.53	29.36	30.22	50.30	33.37	15.41	74.00	2.37	2.34
7	19.95	54.27	33.89	30.22	68.35	49.58	17.45	73.00	2.45	2.41
8	22.89	63.81	40.35	30.22	68.40	46.02	20.35	73.00	2.41	2.39
9	25.25	71.85	46.01	30.22	68.40	42.43	22.76	73.00	2.44	2.41

TCJ - 32.00 TARE --.10 STARE - 1.46 B1 - .966

SCROLL AND GUIDE VANE TESTS OF ICP RADIAL TURBINE

TABLE A3 OUTPUT DATA Run 1

PT	PTC/P1	WVC	PHI	ALPH(1)	V1	T1	MACH1	P1
1	1.088	.798	.8949	80.92	364.81	572.87	.311	30.416
2	1.092	.822	.9030	80.94	377.76	574.26	.322	30.435
3	1.134	.998	.9079	80.93	453.09	571.25	.387	30.594
4	1.232	1.338	.9118	80.83	583.89	561.73	.503	30.947
5	1.289	1.513	.9105	80.68	643.02	559.64	.555	31.138
6	1.340	1.656	.9161	80.69	694.42	555.68	.601	31.348
7	1.393	1.791	.9137	80.57	736.23	553.77	.638	31.486
8	1.463	1.981	.9147	80.45	786.55	546.52	.687	31.751
9	1.521	2.130	.9148	80.36	824.74	542.28	.723	32.015

PROGRAM SCROLL

R.L. BOSHOVEN

SCROLL AND GUIDE VANE TESTS OF ICP RADIAL TURBINE

TABLE A4 INPUT DATA Run 2

PT	DPVC	PUVC	P5P	PATM	HATM	H1	SR	TRM	V4	V5
1	5.23	12.83	7.34	30.20	57.70	54.11	4.85	74.10	1.88	1.85
2	7.57	18.96	10.99	30.20	57.70	52.39	6.63	74.20	1.88	1.87
3	9.83	24.93	14.70	30.20	57.70	50.43	8.36	74.60	1.89	1.88
4	12.02	30.91	18.55	30.20	57.75	48.16	10.15	74.90	1.90	1.89
5	14.45	37.99	23.09	30.20	57.70	45.93	12.27	75.00	1.92	1.94
6	16.91	45.26	27.94	30.20	68.90	54.88	14.44	75.40	1.98	2.00
7	19.74	54.15	33.68	30.20	71.25	53.18	17.15	75.60	2.03	2.07
8	22.06	61.53	38.87	30.20	73.35	53.49	19.33	75.60	2.08	2.13
9	23.07	64.72	41.15	30.20	75.85	53.94	20.42	75.70	2.11	2.16
10	26.96	77.96	50.25	30.20	78.40	53.83	24.35	76.00	2.18	2.24

TCJ - 32.00 TARE---.22 STARE - 1.19 B1 - 1.026

SCROLL AND GUIDE VANE TESTS OF ICP RADIAL TURBINE

TABLE A4 OUTPUT DATA Run 2

PT	PTO/P1	WVC	PHI	ALPH(1)	V1	T1	MACH1	P1
1	1.093	.817	.8883	81.47	368.62	562.96	.317	30.347
2	1.137	1.002	.8973	81.48	446.87	558.54	.386	30.473
3	1.180	1.164	.8964	81.37	506.78	554.22	.439	30.616
4	1.224	1.314	.9003	81.32	561.13	549.84	.488	30.786
5	1.277	1.476	.9026	81.25	617.88	546.47	.539	30.945
6	1.333	1.633	.9007	81.14	668.00	543.75	.585	31.109
7	1.394	1.814	.9091	81.06	724.44	540.29	.636	31.406
8	1.454	1.959	.9019	80.90	762.57	538.22	.671	31.538
9	1.476	2.021	.9087	80.93	783.60	536.83	.690	31.688
10	1.582	2.268	.9013	80.66	841.73	532.48	.744	31.882

PROGRAM SCROLL R.L. BOSHOVEN

SCROLL AND GUIDE VANE TESTS OF ICP RADIAL TURBINE

TABLE A5 INPUT DATA Run 3

PT	DPVC	PUVC	P5P	PATM	HATM	H1	SR	TRM	V4	V5
1	2.50	5.85	3.30	30.16	53.00	50.80	1.85	70.00	1.77	1.71
2	6.67	16.12	9.31	30.16	53.15	46.66	4.74	70.30	1.80	1.77
3	10.04	25.06	14.77	30.16	54.00	43.66	7.38	70.70	1.82	1.81
4	13.44	34.29	20.72	30.16	58.40	43.90	10.13	71.20	1.85	1.85
5	16.31	42.75	26.18	30.16	62.75	44.05	12.73	74.00	1.85	1.85
6	19.37	51.65	32.14	30.16	67.85	44.69	15.40	73.00	1.99	2.00
7	21.69	59.33	37.12	30.16	67.90	40.66	17.92	74.00	1.64	1.72
8	24.53	68.21	43.40	30.16	64.35	32.48	20.50	75.00	1.58	1.63
9	27.22	77.65	49.70	30.16	64.45	26.76	23.23	76.10	1.63	1.66
10	29.18	84.12	54.57	30.16	74.05	32.37	25.27	77.00	1.66	1.69

TCJ - 32.00 TARE - 0 STARE - .22 B1 - .996

SCROLL AND GUIDE VANE TESTS OF ICP RADIAL TURBINE

TABLE A5 OUTPUT DATA Run 3

PT	PTO/P1	WVC	PHI	ALPH(1)	V1	T1	MACH1	P1
1	1.039	.540	.9125	81.36	248.85	562.94	.214	30.218
2	1.108	.918	.9103	81.18	405.55	557.06	.351	30.532
3	1.170	1.166	.9208	81.18	505.54	551.24	.439	30.814
4	1.236	1.395	.9194	81.06	584.81	545.82	.511	31.118
5	1.294	1.585	.9294	81.06	649.95	539.13	.571	31.418
6	1.356	1.771	.9259	80.89	705.86	539.43	.620	31.749
7	1.406	1.949	.9400	80.93	747.97	521.99	.668	32.045
8	1.469	2.136	.9315	80.74	782.37	513.63	.704	32.382
9	1.527	2.311	.9328	80.64	820.67	509.85	.742	32.806
10	1.572	2.435	.9331	80.59	848.13	507.36	.768	33.095

PROGRAM SCROLL R.L. BOSHOVEN

SCROLL AND GUIDE VANE TESTS OF ICP RADIAL TURBINE

TABLE A6 INPUT DATA Run 4

PT	DPVC	PUVC	P5P	PATM	HATM	H1	SR	TRM	V4	V5
1	3.68	8.80	5.04	29.98	48.97	45.77	2.67	68.20	.89	.88
2	7.74	19.07	11.15	29.98	52.05	44.82	5.62	69.00	.91	.90
3	11.53	29.04	17.33	29.98	54.12	42.81	8.54	69.40	.93	.92
4	14.49	37.49	22.75	29.98	58.75	43.82	11.00	69.80	.94	.94
5	17.02	44.72	27.57	29.98	60.60	42.22	13.16	70.00	.96	.96
6	19.71	53.03	32.83	29.98	63.35	41.24	15.65	70.20	.98	.98
7	21.99	60.20	37.82	29.98	66.90	41.15	17.78	70.70	1.00	1.00
8	25.09	70.18	44.55	29.98	70.93	40.02	20.75	71.00	1.02	1.02

TCJ - 32.00 TARE - 0 STARE - .21 B1 - 1.039

SCROLL AND GUIDE VANE TESTS OF ICP RADIAL TURBINE

TABLE A6 OUTPUT DATA Run 4

PT	PTO/P1	WVC	PHI	ALPH(1)	V1	T1	MACH1	P1
1	1.060	.684	.9093	81.76	295.66	523.67	.264	30.117
2	1.131	1.034	.9140	81.64	430.12	516.44	.386	30.411
3	1.202	1.312	.9130	81.46	522.48	510.01	.472	30.710
4	1.262	1.517	.9111	81.34	585.19	505.12	.531	30.975
5	1.314	1.686	.9105	81.24	632.20	501.25	.576	31.228
6	1.370	1.865	.9159	81.16	681.28	496.78	.623	31.501
7	1.422	2.016	.9143	81.06	717.64	493.44	.659	31.767
8	1.489	2.220	.9148	80.93	762.01	488.87	.703	32.145

PROGRAM SCROLL R.L. BOSHOVEN

SCROLL AND GUIDE VANE TESTS OF ICP RADIAL TURBINE

TABLE A7 INPUT DATA Run 5

PT	DPVC	PUVC	P5P	PATM	HATM	H1	SR	TRM	V4	V5
1	3.99	9.51	5.42	29.94	45.80	41.96	2.87	72.00	.98	.97
2	7.80	19.11	11.18	29.94	51.70	43.84	5.64	72.00	.97	.96
3	11.58	29.19	17.34	29.94	56.40	44.04	8.59	72.20	.97	.96
4	14.73	37.76	22.88	29.94	59.62	43.18	11.15	72.30	.98	.98
5	17.18	44.97	27.47	29.94	62.50	42.36	13.32	72.20	.98	.98
6	19.92	53.52	33.17	29.94	64.17	39.64	15.87	72.20	1.00	1.00
7	22.51	61.44	38.48	29.94	69.25	40.38	18.28	72.40	1.01	1.01
8	25.21	70.26	44.72	29.94	73.25	39.43	20.93	72.40	1.01	1.01
9	28.21	80.53	51.71	29.94	77.25	37.38	24.00	72.40	1.01	1.01

TCJ - 32.00 TARE - 0 STARE - .22 B1 - .989

SCROLL AND GUIDE VANE TESTS OF ICP RADIAL TURBINE

TABLE A7 OUTPUT DATA Run 5

PT	PTO/P1	WVC	PHI	ALPH(1)	V1	T1	MACH1	P1
1	1.064	.711	.9143	81.26	306.81	527.14	.273	30.113
2	1.130	1.035	.9177	81.18	431.24	519.05	.386	30.408
3	1.199	1.312	.9218	81.06	525.38	511.55	.474	30.738
4	1.260	1.527	.9202	80.91	589.71	506.47	.534	31.038
5	1.308	1.692	.9255	80.85	637.82	501.55	.581	31.310
6	1.367	1.875	.9266	80.78	687.61	496.95	.629	31.633
7	1.420	2.045	.9281	80.68	727.94	492.65	.669	31.951
8	1.482	2.225	.9269	80.58	767.36	487.74	.709	32.314
9	1.547	2.428	.9289	80.47	807.78	482.44	.750	32.759

APPENDIX B

Scroll Area Distribution

For scrolls with circular cross sections, Eckert [13] has derived an approximate equation for the radius of the cross section as a function of the angle of advance assuming frictionless incompressible flow. If the nomenclature is changed for application to a turbine scroll

$$r = \frac{360° - \delta}{c} + \sqrt{\frac{2 r_1}{c}(360° - \delta)} \quad (\text{ft.}) \tag{B-1}$$

where r_1 is the inside radius of the scroll, δ the circumferential angle of advance measured from the inlet pipe centerline, and c a constant defined by

$$c \equiv \frac{720 \pi V_{\delta 1} r_1}{\mathcal{V}} \quad \left(\frac{\text{deg.}}{\text{ft.}}\right) \tag{B-2}$$

$V_{\delta 1}$ is the tangential velocity component at the inside radius of the scroll, and $\mathcal{V}$ is the volume flow rate at the inlet. Since the radius at the inlet of the existing scroll is r = 0.2083 feet and the radius r_1 = 0.5779 feet, equation (B-1) can be solved for c at $\delta = 0$. The resulting $c = 12,800 \frac{\text{deg.}}{\text{ft.}}$ can then be used to determine r, and hence the cross-sectional areas of the scroll at various δ.

The calculated cross-sectional area of the scroll can be corrected for frictional losses to maintain a constant pressure distribution around the periphery. The ratio of corrected to uncorrected radius is

$$\frac{r_f}{r} \equiv \frac{1}{\sqrt[4]{1 - \Delta q}} \tag{B-3}$$

where Δq is a non-dimensional head loss, defined below, and determined from the empirical relation

$$\Delta q \equiv \frac{2g\Delta H}{V_{\delta 1}^2} = 0.0233 f c r_1 \ln\left[\frac{\sqrt{2r_1 c} + 3\sqrt{360^\circ}}{\sqrt{2r_1 c} + 3\sqrt{360^\circ - \delta}}\right] \quad \text{(B-4)}$$

The skin friction coefficient, f, is estimated to be 0.0025. The corrected area is

$$A_{\delta f} = \frac{A_\delta}{\sqrt{1-\Delta q}} \quad (\text{in.}^2) \qquad \text{(B-5)}$$

The calculated areas are tabulated in Table B1 and the area distribution is shown graphically in Fig. 17.

TABLE B1

δ (deg.)	A_δ (in.^{2})	Δq	$A_{\delta f}$ (in.^{2})
0	19.646	0	19.646
30	17.802	0.0059	17.854
75	15.089	0.0152	15.205
120	12.459	0.0259	12.624
165	9.894	0.0379	10.087
180	9.062	0.0422	9.260
210	7.414	0.0514	7.612
255	5.036	0.0684	5.218
300	2.764	0.0902	2.897
330	1.338	0.1107	1.419
360	0	0.1654	0

APPENDIX C

Data Reduction

Data reduction to obtain scroll and guide vane performance from torque tests was carried out by program SCROLL. Program SCROLL is described in detail in Appendix A. The reduction of data for the other investigations is described below.

C1. Flow Rate Calculation

Flow rates were calculated using the same relations and procedure as described in section A1 of Appendix A for digital computer calculation.

C2. Temperature

The recorded output in milli-volts of the chromel-alumel and iron-constantan thermocouples was directly reduced to temperature using data tabulated in [6] and interpolating for fractions of degrees as necessary.

C3. Pressures

The specific gravities of mercury G_{Hg} and water G_{H_2O} used in the manometers were calculated for control room temperature t_{rm} using equations (A-1) and (A-2) which were obtained from data tabulated in [4].

The absolute static pressure at the manifold inlet, determined from a micromanometer reading, is

$$p_o = \left(p_5' - tare + 2.54\, P_{atm} \right) \frac{G_{Hg}}{13.59} \qquad \text{(C-1)}$$

The absolute total pressure at the manifold inlet is

$$P_{to} = p_o + 2.54(h_{ref} - h_{to})\frac{G_{H_2O}}{13.59} \qquad \text{(C-2)}$$

when the static pressure at the manifold inlet is the reference pressure. Pressures measured on the 96-inch water manometer board are

$$p = p_o + 2.54(h_{ref} - h)\frac{G_{H_2O}}{13.59} \qquad \text{(C-3)}$$

Pressure ratios and differences are calculated as required.

C4. Pressure Probe Survey Data

Fig. C1 and C2 are calibration curves for the three-dimensional probes used in surveys at the rotor discharge section, and vortex chamber, respectively. Although the curves differ from each other, the procedure used to determine actual pressures and flow angles from recorded data is the same. The pitch angle θ is determined from the calibration curve by entering with the pitch angle pressure coefficient $\frac{p_4-p_5}{P_1-p_2}$ that is obtained from measured data. The subscripts refer to the tap on the probe at which the pressure is measured. The positions of these taps are shown in Fig. 11. With the pitch angle θ, the velocity pressure coefficient $\frac{P_t-p_s}{P_1-p_2}$ is established from the calibration curve for the M_r range where M_r is defined as $\frac{P_1-p_2}{P_1\text{(absolute)}}$. Since (P_1-p_2) is measured, the corrected dynamic pressure (P_t-p_s) is determined. The total pressure coefficient

$\frac{P_1 - P_t}{P_t - p_s}$ is very nearly zero in the range of moderate pitch angle, hence the measured total pressure requires no correction. The total pressure was measured against atmospheric pressure, hence total and static absolute pressure, as well as pressure ratios, are obtained by using the prevailing barometer reading.

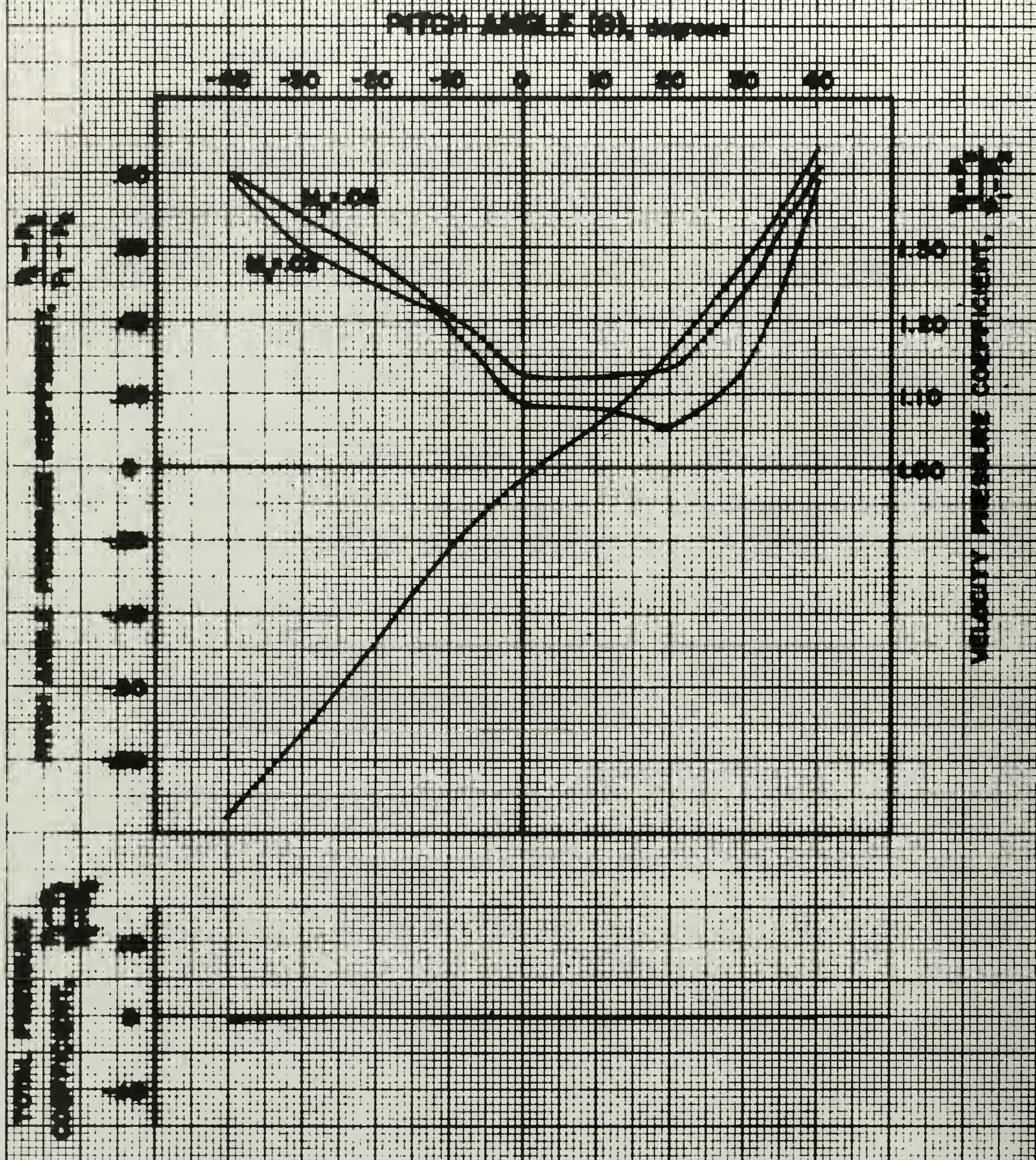

FIG. 21
CALIBRATION OF DA-120 PROBE No. 529

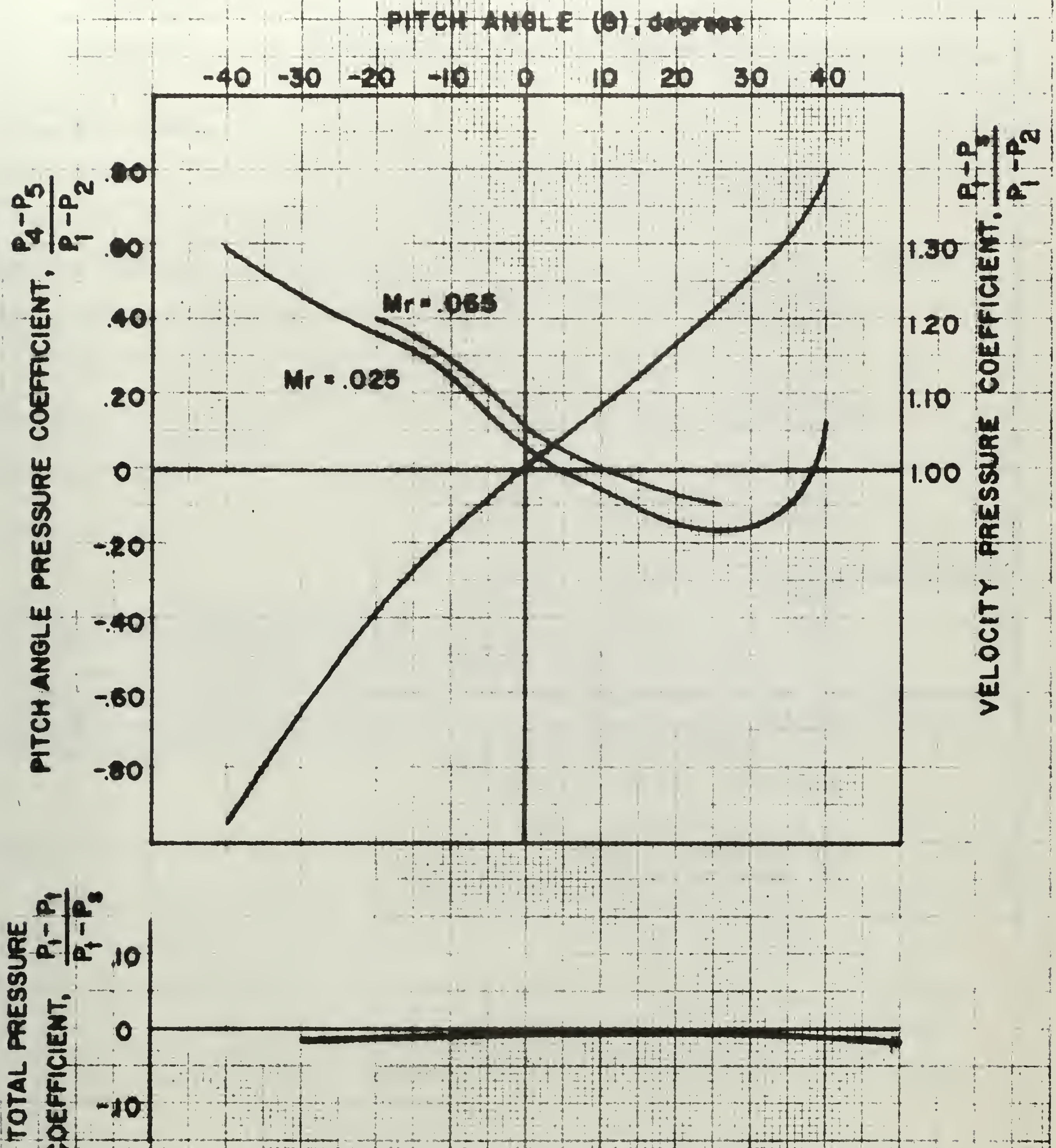

Fig. C2

CALIBRATION OF DA-125 PROBE No. 926

INITIAL DISTRIBUTION LIST

		No. Copies
1.	Defense Documentation Center Cameron Station Alexandria, Virginia 22314	20
2.	Library Naval Postgraduate School Monterey, California 93940	2
3.	Commander, Naval Air Systems Command Department of the Navy Washington, D. C. 20360	1
4.	Chairman, Department of Aeronautics Naval Postgraduate School Monterey, California 93940	1
5.	Dr. M. H. Vavra Department of Aeronautics Naval Postgraduate School Monterey, California 93940	3
6.	Dr. R. E. Reichenbach Department of Aeronautics Naval Postgraduate School Monterey, California 93940	1
7.	LT R. L. Boshoven, USN USS Oriskany CVA 34 FPO San Francisco, California	1

DOCUMENT CONTROL DATA - R&D

(Security classification of title, body of abstract and indexing annotation must be entered when the overall report is classified)

1. ORIGINATING ACTIVITY *(Corporate author)* Naval Postgraduate School Monterey, California 93940	2a. REPORT SECURITY CLASSIFICATION UNCLASSIFIED 2b. GROUP

3. REPORT TITLE

An Investigation of Compressible Flows with Large Whirl Components

4. DESCRIPTIVE NOTES *(Type of report and inclusive dates)*

5. AUTHOR(S) *(Last name, first name, initial)*

BOSHOVEN, Robert L., LT, USN

6. REPORT DATE	7a. TOTAL NO. OF PAGES	7b. NO. OF REFS
June 1967	111	13

8a. CONTRACT OR GRANT NO. b. PROJECT NO. c. d. Unlimited Distribution	9a. ORIGINATOR'S REPORT NUMBER(S) 9b. OTHER REPORT NO(S) *(Any other numbers that may be assigned this report)*

10. AVAILABILITY/LIMITATION NOTICES

~~This document is subject to special export controls and each transmittal to foreign government or foreign nationals may be made only with prior approval of the Naval Postgraduate School.~~

11. SUPPLEMENTARY NOTES	12. SPONSORING MILITARY ACTIVITY
	Naval Postgraduate School

13. ABSTRACT

This investigation was conducted to determine the losses in the scroll and inlet guide vanes of a dual discharge, radial-inflow turbine. Difficulties are encountered in such tests because the air is discharged from the guide vanes with a large whirl component into the cavity normally occupied by the turbine rotor. Connected with such flows are phenomena such as choking and energy separation. This led to the investigation of the flow in a vortex chamber where the vortex is driven by the inlet guide vanes of the radial turbine.

The air tests were conducted at the Turbo-Propulsion Laboratory of the Naval Postgraduate School, Monterey, California.

14. KEY WORDS	LINK A		LINK B		LINK C	
	ROLE	WT	ROLE	WT	ROLE	WT
whirling flow						
vortex chamber						
radial turbine						